

AD-A126 319

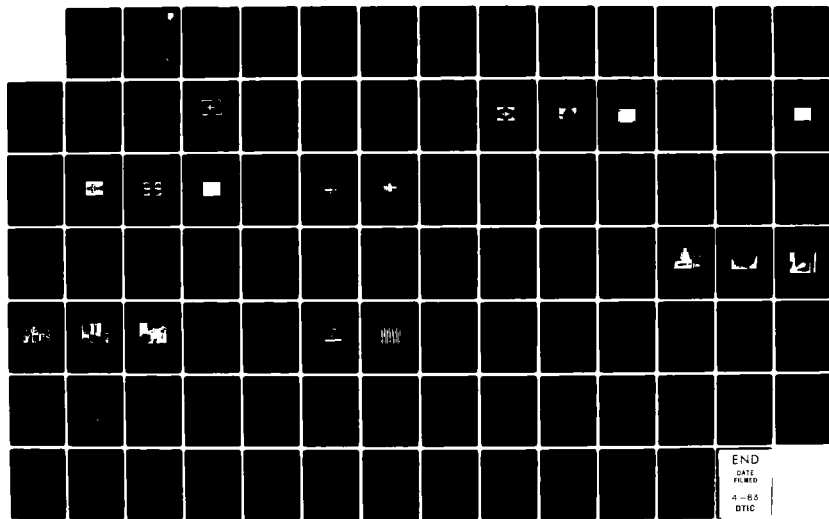
GENERALIZED MATCHED FILTERS(U) AERODYNE RESEARCH INC  
BILLERICA MA H J CAULFIELD ET AL. JAN 83 ARI-RR-320  
RADC-TR-82-329 F19628-80-C-0082

1/1

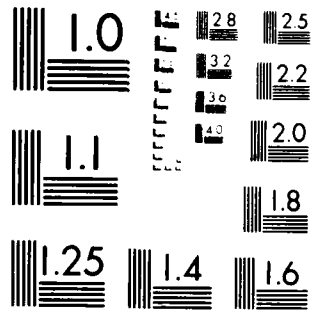
UNCLASSIFIED

F/G 9/5

NL



END  
DATE  
FILMED  
4-85  
DTIC



MICROCOPY RESOLUTION TEST CHART  
NATIONAL BUREAU OF STANDARDS-1963-A

ADA 126319

RADC-TR-82-329  
Final Technical Report  
January 1983

12



# GENERALIZED MATCHED FILTERS

**Aerodyne Research, Inc.**

H. J. Caulfield  
P. F. Mueller  
M. H. Weinberg  
A. H. Epstein

APPROVED FOR PUBLIC RELEASE; DISTRIBUTION UNLIMITED

This effort was funded totally by the Laboratory Directors' Fund

**ROME AIR DEVELOPMENT CENTER  
Air Force Systems Command  
Griffiss Air Force Base, NY 13441**

DTIC  
ELECTE  
APR 4 1983

S

A

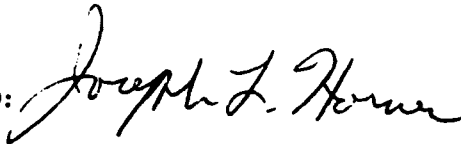
DTIC FILE COPY

03 04 04 049

This report has been reviewed by the RADC Public Affairs Office (PA) and is releasable to the National Technical Information Service (NTIS). At NTIS it will be releasable to the general public, including foreign nations.

RADC-TR-82-329 has been reviewed and is approved for publication.

APPROVED:



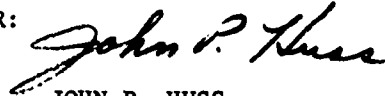
JOSEPH L. HORNER  
Project Engineer

APPROVED:



HAROLD ROTH, Director  
Solid State Sciences Division

FOR THE COMMANDER:



JOHN P. HUSS  
Acting Chief, Plans Office

If your address has changed or if you wish to be removed from the RADC mailing list, or if the addressee is no longer employed by your organization, please notify RADC (ES0) Hanscom AFB MA 01731. This will assist us in maintaining a current mailing list.

Do not return copies of this report unless contractual obligations or notices on a specific document requires that it be returned.



UNCLASSIFIED

SECURITY CLASSIFICATION OF THIS PAGE(When Data Entered)

optical means. Instead, it requires a computer generated hologram. Because no adequate computer hologram existed, Aerodyne built such a "holowriter". Its performance, relative to the prior state of the art, is shown below:

<u>Parameter</u>	<u>Holowriter</u>	<u>Prior Art</u>
(1) Absolute Location Accuracy of Picture Elements	$1:10^6$	1:250
(2) Picture Elements In One Direction	$1.4 \times 10^4$	$2 \times 10^3$
(3) Total Number Of Picture Elements	$2 \times 10^8$	$4 \times 10^6$

UNCLASSIFIED

SECURITY CLASSIFICATION OF THIS PAGE(When Data Entered)

TABLE OF CONTENTS

<u>Section</u>		<u>Page</u>
1	INTRODUCTION .....	1-1
	1.1 Purpose of the Study .....	1-1
	1.2 Results of the Study .....	1-1
2	HOLOGRAM DESIGN .....	2-1
	2.1 Introduction .....	2-1
	2.2 Digital Generalized Matched Filter Demonstration .....	2-6
	2.3 Discussion .....	2-22
	2.4 References .....	2-25
3	HOLOGRAM CONSTRUCTION .....	3-1
	3.1 Characterizing the Need .....	3-1
	3.2 Consequences of the Hologram Writer for Hologram Encoding .....	3-3
	3.3 Basic Scheme of the Holowriter .....	3-4
4	DESIGN CONSIDERATION .....	4-1
	4.1 Introduction .....	4-1
	4.2 Temperature of Room .....	4-1
	4.3 Stage Motion .....	4-2
	4.4 Photographic Plate Choice .....	4-4
	4.5 CRT Choice .....	4-4
	4.6 Mirror Design .....	4-5
	4.7 Vibration .....	4-6
	4.8 Air Currents .....	4-6
	4.9 Interferometer .....	4-7
	4.10 Radio-Frequency Interference .....	4-7
	4.11 Information Flow .....	4-7
5	SYSTEM DESCRIPTION .....	5-1
	5.1 Introduction .....	5-1
	5.2 System Appearance .....	5-1
	5.3 Alignment, Magnification, and Focus .....	5-1
	5.4 Final System Specifications .....	5-8
	5.5 Time Budget For One Cell .....	5-8
	5.6 Sample Rulings .....	5-9

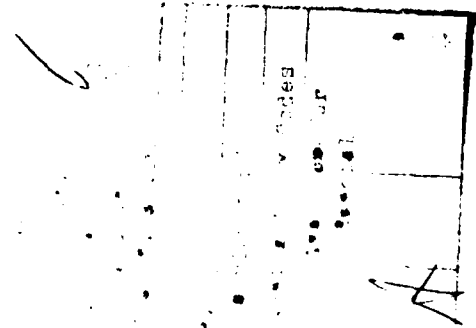


Table of Contents (Continued)

<u>Section</u>	<u>Page</u>
APPENDIX A DETAILED PROCEDURE FOR CALCULATING THE GMF	A-1
APPENDIX B THERMAL EXPANSION COMPENSATION	B-1
APPENDIX C PHOTOGRAPHIC PLATE	C-1
APPENDIX D HOLOGRAM DISPLAY GENERATOR	D-1

LIST OF ILLUSTRATIONS

<u>Figure</u>		<u>Page</u>
2.1	Ramtek Display of the Hand-Drawn Aircraft Used in These Experiments .....	2-7
2.2	Notation Used to Designate the Magnification ( $m$ ) and Rotation Angle ( $\theta$ ) for the Inputs Referred to in Figures 2.3 through 2.10 .....	2-9
2.3	Horizontal Traces Through the Correlation Peaks With the Inputs As in Figure 2.2 and the Filter Matched to $e$ ( $m = 1, \theta = 0^0$ ).....	2-10
2.4	Vertical Traces As in Figure 2.3.....	2-11
2.5	Ramtek Display of the Correlation Plane Corresponding to $e$ in Figure 2.2 .....	2-12
2.6	Ramtek Display of the Filter Matched to $e$ of Figure 2.2.....	2-13
2.7	Ramtek Display of the GMF Which Groups All Nine Inputs of Figure 2.2.....	2-14
2.8	Horizontal Traces Through the GMF Correlation Planes Corresponding to the Various Inputs of Figure 2.2.....	2-15
2.9	Vertical Traces As in Figure 2.8.....	2-16
2.10	Ramtek Display of the Correlation Plane of the GMF With $e$ of Figure 2.2 As Input.....	2-17
2.11	The Squared Magnitude of the Complex Image to Which the GMF is "Matched".....	2-19
2.12	Ramtek Display of the Correlation Plane Created By the Filter Matched to $e$ in Figure 2.2 When the Input is $C$ .....	2-20
2.13	Equivalent of Figure 2.12 With the GMF.....	2-21
2.14	The Correlation Plane for the $m = 1$ CMF With $m = 1$ Input....	2-23
2.15	The Correlation Plane for the $m = 1$ CMF With $m = 0.8$ Input..	2-24

List of Illustrations (Continued)

<u>Figure</u>		<u>Page</u>
3.1	Schematic Drawing of the Primary Components of the Holowriter .....	3-5
4.1	Simplified Information and Control Flow Diagram .....	4-9
5.1	The CRT, Microscope, and Interferometer are Shown here on the Air Suspended Granite Table .....	5-2
5.2	Environmental Control Station .....	5-3
5.3	One of the Insulated Metal Doors to the Temperature Controlled Room .....	5-4
5.4	Adjacent-to-the Room Electronics .....	5-5
5.5	Aerodynes Prime 400 Computer System .....	5-6
5.6	The Ramtek Display (a) is interfaced to the Prime through Special Boards Designed and Built at ARI .....	5-7
5.7	A 7 cm x 7 cm Ronchi Ruling Written with the Holowriter.....	5-10
5.8	A Magnified Image of a Portion of the Figure 5.7 showing 10 $\mu$ m lines .....	5-11

## 1. INTRODUCTION

### 1.1 Purpose of the Study

This study was based on the hope that we could utilize the power of the computer to both design and construct pattern recognition holograms. At the beginning of this study the only computer designs were limited to 80 picture elements (pixels) in the hologram plane<sup>1</sup> and computer hologram writers were limited to a few million total pixels with positional accuracy of roughly one part in a hundred (or worse) in each direction. Accordingly, our goals were to:

- o Computer design holograms of arbitrary size (number of pixels) optimized for any selectable goal and
- o Construct a computer hologram writer capable of one part in a million location accuracy and capable of writing  $10^8$  to  $10^9$  pixels.

### 1.2 Results of the Study

Both goals were met. As a result we can now design and construct the optimum hologram for any reasonable task. This appears to be a revolutionary advance over the prior art in which some ad hoc optimization of optical holograms was possible,<sup>2</sup> but no systematic approach to full optimization in either design or construction was available.

As this work progressed, it became obvious that computer optimization of optical masks was possible in principle and that the optimization mathematics (eigenvector/eigenvalue solutions) was subject to optical solution. We believe that these two realizations are important but not key to our primary results. Accordingly, they are relegated to appendices.

## 2. HOLOGRAM DESIGN

### 2.1 Introduction

The use of statistically-derived optical filters has been discussed by many authors over the past several years.<sup>1-4</sup> One of the methods discussed was called the "generalized matched filter" or GMF because it reduces to the matched filter for simple enough situations (very simple invariant objects in colored noise) the GMF gives different results. The basic idea is to view the  $M \times N$  complex feature vector and use the classical statistical method of linear discriminant analysis to find that linear combination of the  $MN$  samples which best separates (in an expected-value sense) the class of images of interest from all other images and noise. Thus all "uninteresting" images of interest from all other images and noise. Thus all "uninteresting" images and noise are lumped together according to their probability of occurrence to form the set of images against which we seek to discriminate.

The basic ideas are easy to express mathematically. Any input scene  $f(x,y)$  will produce a Fourier transform pattern  $F(u,v)$ . In discrete terms, the Fourier transform samples can be written

$$F_{mn} = F(m\Delta u, n\Delta y), \quad (1)$$

where

$$0 > m > M,$$

$$0 > n > N,$$

$\Delta u$  = sampling spacing in the  $u$  direction, and

$\Delta v$  = sampling spacing in the  $v$  direction.

We then label the  $F_{mn}$ 's in any unique but arbitrary fashion, e.g.

$$G_1 = F_{11}$$

$$G_2 = F_{12}$$

⋮

$$G_N = F_{1N}$$

$$G_{N+1} = F_{21}$$

$$G_{N+2} = F_{22}$$

⋮

$$G_{2N} = F_{2N}$$

$$G_{2N+1} = F_{31}$$

⋮

$$G_{MN} = F_{MN}$$

(2)

This reordered  $F_{mn}$  matrix becomes the vector

$$\vec{G} = (G_1, G_2, \dots, G_{MN})^T \quad (3)$$

We then seek an MN component vector

$$\vec{C} = (C_1, C_2, \dots, C_{MN})^T \quad (4)$$

such that the numbers

$$\begin{aligned} P &= \vec{C} \cdot \vec{G} \\ &= C_1 G_1 + C_2 G_2 + \dots + C_{MN} G_{MN} \end{aligned} \quad (5)$$

separate into one set  $\{P_T\}$  for the desired set of targets and another set  $\{P_{CN}\}$  and  $\{P_{CN}\}$  are "optimally" separated. Our definition of optimality is chosen for mathematical tractability. We choose C such that

$$R = \frac{\vec{C}^T B \vec{C}}{\vec{C}^T W \vec{C}} \quad (6)$$

is maximized. The "between-class scatter matrix" B is given by

$$\underline{B} = \sum_{i=1}^2 N_i [\vec{G}_i - \langle \vec{G} \rangle] [\vec{G}_i - \langle \vec{G} \rangle]^T \quad (7)$$

where

$N_1$  = number of entries in  $\{P_T\}$ ,

$N_2$  = number of entries in  $\{P_{CN}\}$ ,

$\vec{G}_1$  = mean G for  $\{P_T\}$ ,

$\vec{G}_2$  = mean G for  $\{P_{CN}\}$ , and

$\langle \vec{G} \rangle$  = mean G for the entire data set.

The "within-class scatter matrix" is given by

$$\underline{W} = \underline{W}_1 + \underline{W}_2 \quad (8)$$

where

$$\underline{W}_1 = \sum_{i=1}^{N_1} (\vec{G}_{1,i} - \vec{G}_1)(\vec{G}_{1,i} - \vec{G}_1)^T$$

$$G_{1,i} = i^{\text{th}} / \vec{G} \text{ vector in } \{P_T\}, \quad (9)$$

$$\underline{W}_2 = \sum_{i=1}^{N_2} (G_{2,i} - G_2)(G_{2,i} - G_2)^T, \text{ and}$$

$$G_{2,i} = i^{\text{th}} / \vec{G} \text{ vector in } \{P_{CN}\}. \quad (10)$$

Differentiating Equation (2-6) with respect to  $\vec{C}$  leads to a generalized eigenvalue problem of the form

$$[\underline{B} - \lambda \underline{W}] \underline{C} = 0 \quad (11)$$

The eigenvector with the highest eigenvalue  $\lambda$  is the  $\vec{C}$  whose components define the CMF.

Clearly a 256 x 256 CMF requires solution of a generalized eigenvalue problem with 65536 x 65536  $\underline{B}$  and  $\underline{W}$  matrices. Our initial computer program allowed us to solve 80 x 80 problems, e.g. and 8 x 10 CMF. We know of no general methods to solve such large eigenvalue problems. The primary goal of this paper is to observe that the ratio of the determinant of the between-class matrix is maximized. Here

$E[P_x]$  = expected value of P for an input in set {x} where

x = T or CN and

$\sigma_x$  = standard deviation of P values for inputs of set {x}.

In words, we want to optimize the T/CN separation relative to the tightness of their clustering. A more precise statement is available elsewhere.<sup>5</sup>

The vector  $\vec{C}$  is then retranslated into a two-dimensional format. The mn component of C is the transmission of the GMF at  $m\Delta u$  and  $n\Delta y$ .

The purposes of this paper are to show that:

- (1) Very large MN values can be handled quite easily if we arbitrarily assume

$$E[(P_k - \bar{P}_k) * (P_l - \bar{P}_l)] = \delta_{kl} \quad (12)$$

where

$$\bar{P}_k = E(P_k) \quad ,$$

$$\bar{P}_\ell = E(P_\ell) \quad ,$$

$$\delta_{k\ell} = \begin{cases} 1 & \text{if } k = \ell \\ 0 & \text{if } k \neq \ell \end{cases} \quad ,$$

and \* indicates complex conjugation;

- (1) The calculation problem can be simplified tremendously by assuming that the individual components of  $G$  have no cross correlations and hence that  $\underline{B}$  and  $\underline{W}$  are diagonal,
- (2) This assumption leads to very useful GMF's relative to some, not necessarily all, of the alternatives,
- (3) The GMF correlation peaks so calculated are one-pixel wide (as opposed to the auto-correlation pattern produced by the MF or matched filter which is twice the diameter of the object).

Thus this is intended to demonstrate GMF calculation and operation. A fair and statistically-useful comparison of all the available pattern recognition filters would be desirable but is well beyond the scope of this paper.

## 2.2 Digital Generalized Matched Filter Demonstration

To demonstrate the digital GMF we used a binary, hand-drawn silhouette of an airplane on a 128 x 128 grid. Figure 2.1 shows a display of the airplane on a Ramtek graphic display system. The nature of the Ramtek display is such that a square input is displayed as a rectangular output with 14 units horizontally for each 10 units vertically. We will use this display to produce color and black and white representation of the images generated during our digital experimentation. We have chosen to concentrate on

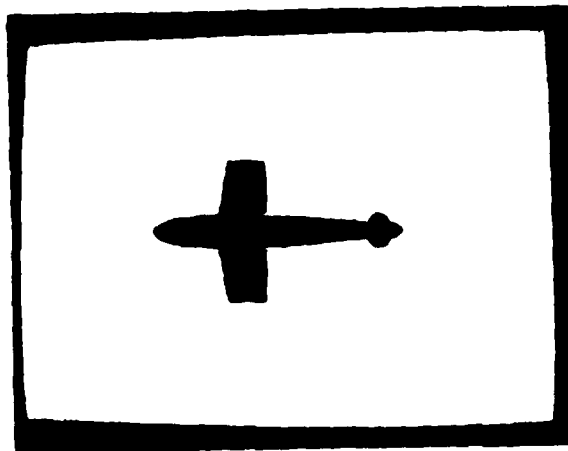


Figure 2.1. Ramtek Display of the Hand-Drawn Aircraft Used in These Experiments

reduction of within-class variability of filter response as a first demonstration of two-dimensional GMF's. Therefore, we worked with both scale and rotation variations of that input pattern. The pattern was magnified and rotated by digital means through a range of magnifications and rotation angles indicated in Figure 2.2. Figure 2.2 will be important because we will use that same display format to compare CMF with with matched filter results later in this paper.

To produce the generalized matched filter we use as the set of objects that we wish to put in the same class the nine magnification and rotation combinations of Figure 2.2. We created a GMF which best separated this set of airplanes from a second set of inputs comprising Gaussian noise of zero mean and standard deviation equal to that of one tenth the magnitude of the peak of the Fourier transform of the unit magnification, zero rotation Fourier transform. We then generated the generalized matched filter using at each point in the 128 x 128 Fourier transform plane the nine Fourier transform components as well as the 128 x 128 array of white noise samples as described in detail in the Appendix. The filter was generated by assuming that there was no cross correlation between any two points in the Fourier transform plane. This is demonstrably not the case, but handling the general case of covariance matrices with off-diagonal term and the very large sizes encountered in our problem would be impossible with existing equipment. It would involve solving an eigenvector problem of the form of Equation (6) for the  $(128)^2$  points in the Fourier transform plane. Our simplification allows us to treat the problem in conveniently-sized pieces as detailed in the appendix.

We shown in Figures 2.3 and 2.4 horizontal and vertical traces through the correlation points produced by using the matched filter to the  $M = 1, \theta = 0^0$  scene. Figure 2.6 shows the magnitude squared of the matched filter.

	1.1	A	B	C
	1.0	D	E	F
M	0.9	G	H	I
		-7.5°	0°	7.5°
		θ		

Figure 2.2. Notation Used to Designate the Magnification (m) and Rotation Angle ( $\theta$ ) for the Inputs Referred to in Figures 2.3 through 2.10

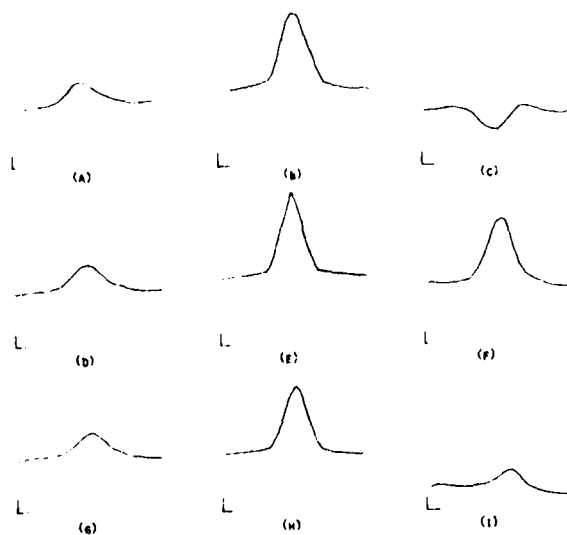


Figure 2.3. Horizontal Traces Through the Correlation Peaks With the Inputs as in Figure 2.2 and the Filter Matched to e ( $m = 1, \theta = 0^0$ ).

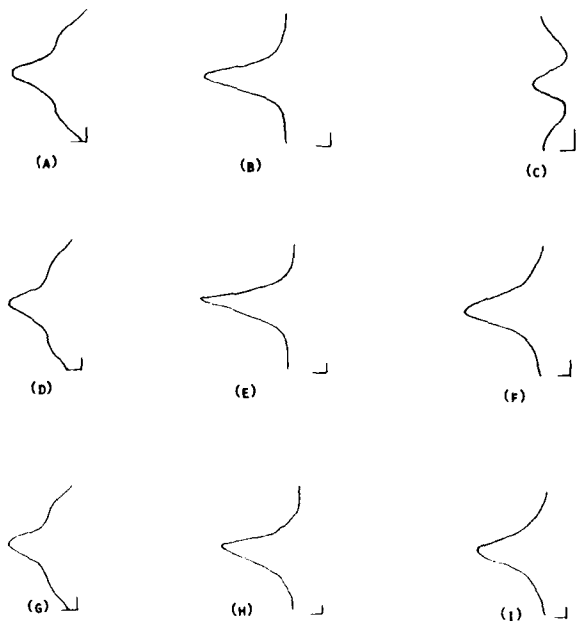


Figure 2.4. Vertical Traces as in Figure 2.3

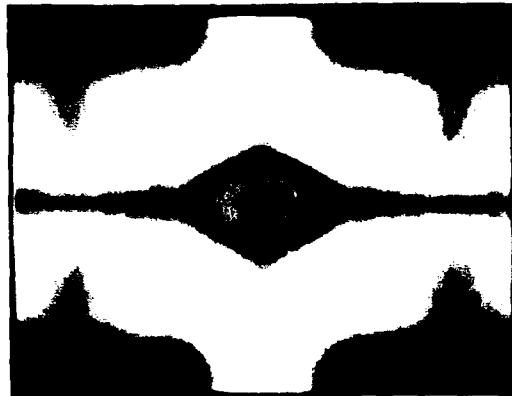


Figure 2.5. Ramtek Display of the Correlation Plane Corresponding to  $e$  in Figure 2.2.



Figure 2.6. Ramtek Display of the Filter Matched to  $\sigma$  of Figure 2.2

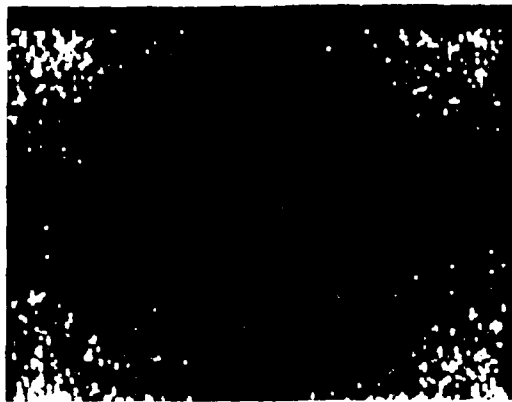


Figure 2.7. Ramtek Display of the GMF Which Groups All Nine Inputs of Figure 2.2

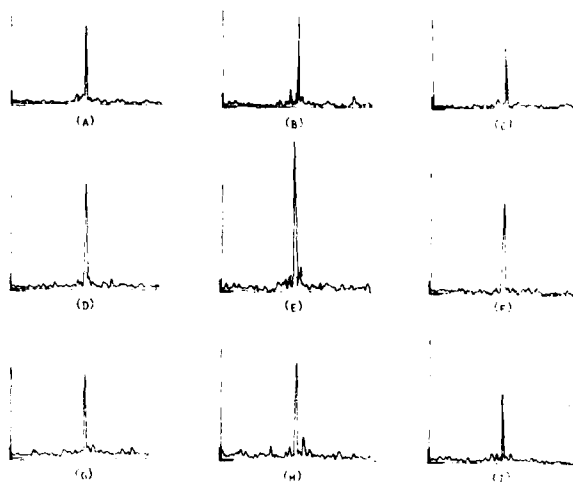


Figure 2.8. Horizontal Traces Through the GMF Correlation Planes Corresponding to the Various Inputs of Figure 2.2

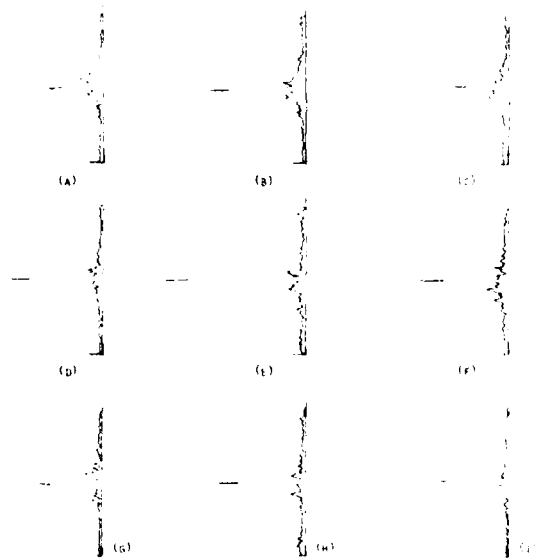


Figure 2.9. Vertical traces as in Figure 2.8



Figure 2.10. Ramtek Display of the Correlation Plane,  $\sigma = 0.01$ , with  $\sigma = 0.01$  Figure 2.2 as Input.

We can now compare these with the GMF results. The GMF designed to group all nine of the images into one class is shown in Figure 2.7. The horizontal and vertical traces through the correlation peaks are shown in Figures 2.8 and 2.9. Figure 2.10 shows the "correlation plane" produced by the  $m = 1$ ,  $\theta = 0^\circ$  input and the GMF.

It is interesting to compare the magnitude squared plots of the  $m = 1$ ,  $\theta = 0^\circ$  matched filter (Figure 2.9) with the magnitude squared of the GMF (Figure 2.10). Clearly the GMF utilizes high spatial frequencies preferentially. By complex conjugation followed by inverse Fourier transformation operating on the matched filter for the  $m = 1$ ,  $\theta = 0^\circ$  case, we recreate the original scene (Figure 2.1). Applying the same sequence of operations to the GMF leads to a new scene which is largely real but has significant negative portions. The squared magnitude of that scene is shown in Figure 2.11. Here we see even more detail of those features which are most useful in recognizing the nine input images and distinguishing them from white noise.

Yet another way of illustrating GMF behavior is to compare the GMF correlation plane with the correlation plane produced by the  $m = 1$ ,  $\theta = 0^\circ$  input case (Figures 2.5 and 2.10). In Figures 2.12 and 2.13 we show the  $m = 1.1$ ,  $\theta = 7.5^\circ$  case. Here the advantage of the GMF in object location is quite obvious. In every case the GMF gives a narrow peak centered on the airplane center of mass. The matched filter always gives a much broader peak and that peak may not be centered properly. Indeed we may have multiple, improperly-located, broad peaks.

Having exercised the GMF to achieve a broad case (all nine  $m$ ,  $\theta$  combinations), we then exercised it to achieve high separability. For this case, we kept  $\theta = 0$  and used magnifications 0.8, 1.0, 1.1, and 1.2. We produced five GMF's each designed to recognize one magnification and discriminate against the others. Here, matched filters do very poorly, see Figures 2.3 and 2.4 for example, but, alternative filters have been suggested

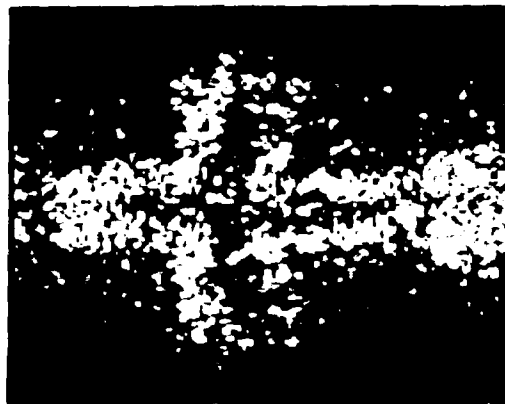


Figure 2.11. The Squared Magnitude of the Complex Image to Which the GMF is "Matched"



Figure 2.12. Ramtek Display of the Correlation Plane Created By the Filter Matched to e in Figure 2.2 When the Input is C

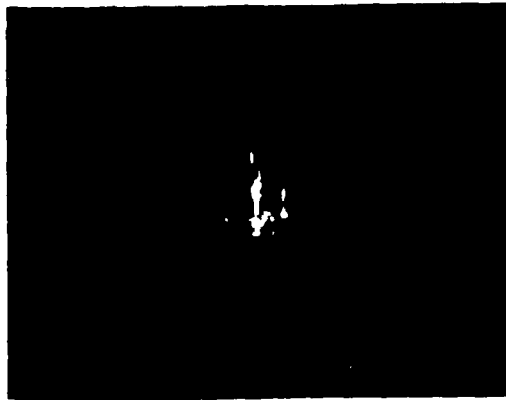


Figure 2.13. Equivalent of Figure 2.12 with the GNF

by Caulfield and Maloney.<sup>3</sup> Thus, we will compare the GMF's with the Caulfield-Maloney filters (CMF's). The Caulfield-Maloney filters (CMF's) are linear combinations of filters matched to the five differently magnified images. The weights are so chosen that the response to the CMF for one image, say the  $m = 1$ , image is high but the response to any other  $m$  is zero (at the centroid of the image). In this sense (contrast between "true" and "false"), the CMF is optimum. Figure 2-14 shows the correlation plane produced by the  $m = 1$  CMF with the  $m = 1$  input. Figure 2-15 shows the correlation plane with the same CMF but  $m = 0.8$  input. The CMF, though, is defined only for a finite set of inputs whereas the GMF is defineable for infinite stochastic sets. Thus the GMF is more versatile. In addition, only the GMF simultaneously optimizes between-class and within-class separations.

### 2.3 Discussion

Generalized matched filters appear to be more flexible than matched filters (no flexibility) or Caulfield-Mahoney filters (useful only for increasing between-class discrimination). Not included in our study was the within-class filters due to Hester and Casasent.<sup>4</sup> The latter authors allude to the possibility of combining their work with what amounts to the Caulfield-Maloney work to achieve full flexibility. Leger et al.<sup>5</sup> also used statistical methods to develop quite different spatial filters with much flexibility. Likewise, Caulfield et al.<sup>6</sup> showed how to weight matched filters to have full flexibility, i.e., with-class and between-class control.

This paper contains the first demonstration that GMF's can be derived for very-general two-dimensional scenes. It shows, as well, the quite-general property that GMF correlation peaks are much narrower than the corresponding classical cross correlation peaks produced by matched filters. This results from the different senses in which matched filters and GMF's are optimized.<sup>2</sup>

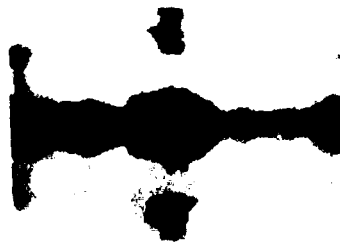


Figure 2.14. The Correlation Plane for the  $m = 1$  CMF with  $m = 1$  Input

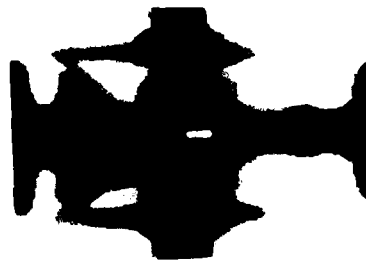


Figure 2.15. The Correlation Plane for the  $em = 1$  CMF with  $m = 0.8$  Input

Of all the matched filter replacements, only the GMF absolutely requires computer recording. On the other hand, all of the methods require computer calculation.

Computer recording to the required accuracies is beyond the capabilities of available hologram writers. We are, however, developing a hologram writer which is capable of writing  $10^6$  and  $10^6$  points to an absolute spatial accuracy of one part in  $10^6$ .<sup>7</sup> A more subtle problem is the fact that optical systems do not necessarily perform good Fourier transforms. Indeed because MTF's degrade off-axis, real systems are space-variant. The GMF has the potentiality of creating the statistically-optimum space-invariant filter for that space-variant system. In addition, matching the spacing of the filter to the exact size spacing and orientation required for the optical equivalent of our digital matching can be a problem. Because the GMF emphasises the high spatial frequency domain, we might expect it to be more sensitive to angular alignment than the matched filter. This will be the case in many circumstances. In our case, however, the exact opposite is true. The angular insensitivity to alignment of the filter comes about from the fact that the GMF was designed to be relatively insensitive to rotation between the input and the filter. It is clear that we could as well design the filter to be insensitive to translation error. Each new insensitivity we add must be expected to cost us something in terms of between-class discrimination, so we have avoided adding that translation insensitivity to this particular filter. We are currently at work on the synthesis of computer generated GMF's and hope to report on that in the near future.

#### 2.4 References

1. H.J. Caulfield and D. Casasent, Opt. Eng. 19, 152 (1980).
2. H.J. Caulfield and R. Haimes, Appl. Opt. 19, 181 (1980).
3. H.J. Caulfield and W.T. Maloney, Appl. Opt. 8, 2354 (1969).

4. C.F. Hester and D. Casasent, Appl. Opt. 19, 1758 (1980).
5. J.R. Leger and S.H. Lee, J. Opt. Am. 72 566 (1982) and Z.C.H. Gu, J.R. Leger, and S.H. Lee, J. Opt. Soc. Am. 72, 787 (1982)
6. H.J. Caulfield, R. Haimes, and J. Horner, Israel J. of Technol. 18, 263 (1980).
7. H.J. Caulfield, P.F. Mueller, D. Dvore, J. Loomis and W. Friday, Proc. Soc. Photo-Opt. Instrum. Eng. 306, (1981).

### 3. HOLOGRAM CONSTRUCTION

#### 3.1 Characterizing the Need

Here we seek to define the necessary characteristics of a hologram writer for practical pattern recognition. The primary quantities are

- o  $N$  (the number of pixels that can be written in each direction),
- o  $p$  (the size of the individual pixel), and
- o  $\delta p$  (the maximum absolute accuracy of the separation of pixels  $p$  and  $N$ ).

Note that perfect optical magnification or demagnification leaves  $N$  unchanged while changing  $p$  to  $mp$  and  $\delta p$  to  $m\delta p$ . Accordingly the most fundamental properties of the writer are  $N$  and  $p/\delta p$ . Nevertheless since demagnification may lead to distortion which must be precompensated for in hologram design, it is important to have  $\delta p$  small enough to produce a usable hologram directly. It is not necessary that  $\delta p$  be small enough to introduce a big splitting angle, because we can use the object wavefront from the computer generated hologram with a separately-derived reference beam to form an optical hologram with any angle.

Thus we can arrive quickly at a minimum value for  $N$ . We know that an off-axis hologram of wavefront  $M$  pixels across requires at least  $4M$  pixels. Very good lenses give as many as 10,000 pixels, so an off-axis hologram for use with a good lens might require  $N > 40,000$ . Most lenses we consider for optical pattern recognition are not that good, so we do not need such large  $N$ . Nevertheless,  $N = 40,000$  is safe.

It is also easy to set the fringe width  $p$  with some accuracy. For the greatest ray deviation to be  $\theta$ , we need to be able to write fringes of width

$$p \approx \frac{\lambda}{4 \sin(\theta/2)} \quad (13)$$

For small  $\theta$ ,

$$p \approx \frac{\lambda}{2\theta} \quad (14)$$

For a reasonable splitting angle like  $\theta = 0.1$  ( $\sim 5.7^\circ$ ) and  $\lambda = 0.6 \mu\text{m}$  (red), we have  $p \approx 3 \mu\text{m}$ . Thus  $p \approx 3 \mu\text{m}$  is a reasonable goal.

To represent an ideal wavefront to  $\lambda/Q$  accuracy, we require  $2\delta w$  (which corresponds to the representation of a full wave) to be represented to 1:Q accuracy, i.e.

$$\frac{p}{\delta p} > Q/2 \quad (15)$$

For a very good hologram  $\lambda/20$  accuracy seems appropriate.

Therefore we start with goals of

$$\begin{aligned} N &\sim 40,000, \\ p &\sim 3 \mu\text{m}, \text{ and} \\ \delta p &\sim 0.3 \mu\text{m}. \end{aligned}$$

Anticipating what follows, the hologram writer we produced has

$$\begin{aligned} N &= 14,000, \\ p &= 5 \mu\text{m}, \text{ and} \\ \delta p &= 0.15 \mu\text{m}. \end{aligned}$$

Note that it is within a factor of 2 to 3 of ideality on all counts and better than need be on  $\delta p$ . As the goals themselves are inexact, we conclude that the

hologram writer we have constructed will be adequate for all or almost all future needs for computer generated pattern recognition holograms.

### 3.2 Consequences of the Hologram Writer for Hologram Encoding

The capabilities of the hologram writer change the way we think of hologram encoding. Because  $Np/\delta p = (1.6 \times 10^4 \times 5)/0.15 \approx 5 \times 10^5$ , as opposed to the more common  $10^3$ , the "phase quantization" problem which has plagued prior computer holograms is effectively negligible. Because  $N$  is substantially larger than before, many more shades of gray (proportional to  $N^2$ ) can be recorded for a given number of object wavefront pixels than ever before. Consider one of the prior-art CRT writers with  $p/\delta p \approx 1$  at smallest  $p$  and  $N = 2000$ . If we want to represent 400 object wavefront pixels, we have a  $4 \times 4$  cell for each. The cell center can have one of four possible positions yielding  $\lambda/4$  accuracy. The cell power transmission can vary from 0 to 1 in 16 steps. With our writer we have a  $32 \times 32$  cell for each or 1024 shades of gray. The phase accuracy is  $\lambda/(32 \times p/\delta p) \approx \lambda/100$ . In the prior art  $\lambda/1000$  accuracy would require an  $M = 2$  hologram (a 2 pixel  $\times$  2 pixel object wavefront). Likewise 1024 shades of gray ( $32 \times 32$  cells) would allow only a 64 pixel by 64 pixel object wavefront. Clearly the new hologram writer obviates many of the tradeoff needs necessitated by previous writers.

Now that computer holography is a serious alternative, we must study some practical issues which were previously ignored. An example of such a consideration is lens imperfection. Perhaps the easiest way to map this is to use the actual optical set up to Fourier analyze a square input. Locations of the peaks and valleys of the power spectrum (uniformly - spaced in the ideal case) will not be uniform. This permits us a peculiar sort of "distortion" measurement. We then determine whether or not this "distortion" is invariant to:

- o Input position (space invariance) and
- o Size of the square (should we call this "distortion invariant distortion"?).

We can then check to see if the power readings follow the ideal "sinc squared" pattern and whether the power pattern is space invariant or "distortion invariant." Armed with these nonideal properties we can design the space invariant hologram optimum in some stochastic sense (Bayes, minimax, etc.) for the system.

### 3.3 Basic Scheme of the Holowriter

The basic scheme is to:

1. Use an ultra-low distortion CRT (greatly demagnified) to write a small, square portion (cell) of the hologram onto a photographic emulsion on an ultraflat photographic plate,
2. Translate the plate to write the next cell,
3. Measure the translation to an absolute accuracy of  $0.1 \mu\text{m}$  interferometrically,
4. Write the next cell on the CRT face with position chosen to compensate for the unpredictable (to within a few microns) stopping position of the stage.

Of course such a system must be computer controlled. Achieving meaningful  $0.2 \mu\text{m}$  accuracies requires extremely careful engineering as well as the use of a temperature controlled room.

Figure 3.1 shows the overall system layout schematically. At least a dozen factors converge to make improvements beyond this performance level very difficult and very expensive. A few of those factors follow:

- i. The special right-angle mirror required for the 2-D, orthogonal interferometry can not be made much longer without itself introducing  $0.1 \mu\text{m}$  errors,

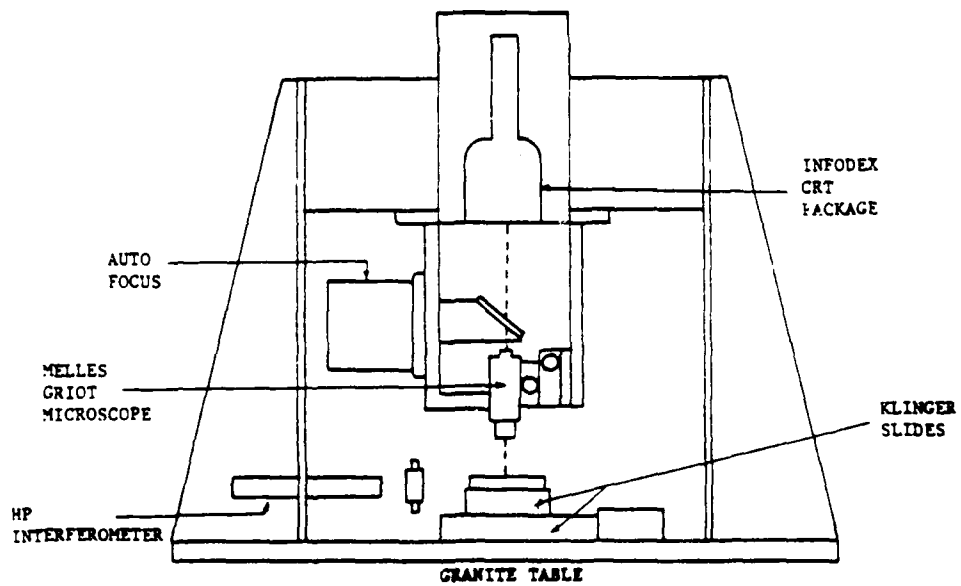


Figure 3.1. Schematic Drawing of the Primary Components of the Holowriter.

2. The writing time for a  $10^6 \times 10^6$  hologram is approaching a full working day and system stability for longer exposures is doubtful (to say nothing of latent image failure),
3. Only one commercial photographic plate exceeds minimum requirements on sensitivity, resolution, and flatness even with the present design,
4. The demagnification is already so great that it, not depth of focus, drives us to use state-of-the-art controllers of lensplate distance,
5. Temperature gradients (beyond those already sensed and compensated for) as well as temperature drift limit mechanical measurement accuracies to no better than about  $0.15 \mu\text{m}$ ,
6. Temperature variations within the room limit the CRT demagnification to roughly its present value.

## 4. DESIGN CONSIDERATIONS

### 4.1 Introduction

Designing the holowriter required the careful selection of components and equally-careful attention to the environment in which those components must function. In this section we describe those considerations.

### 4.2 Temperature of Room

The primary effect of changing room temperature is to change the physical dimensions of all of the metal components, bases, and supports. Listed below are some of the ways we can expect those dimension changes to cause problems:

- o The demagnification factor may vary because the object distance and image distance (relative to the principal planes of the microscope) may change as the basic structure shrinks or expands,
- o The lateral position of the optical axis of the microscope may change relative to the CRT and/or relative to the stage, and
- o The separation between the interferometer and the mirror it is measuring may be due partially to mirror motion and partially to temperature-induced changes in system (e.g. baseplate dimensions).

There are only four ways to combat this problem: design in temperature compensation, minimize temperature change, use non-expanding materials, and measure temperature and correct for it.

Compensation "constancy" was achieved by building the system in a temperature controlled room. We also kept most heat sources (except the CRT) outside that room. There the questions are: how stable is the temperature over the anticipated writing times and how big are the temperature gradients?

Low expansion materials (e.g. special ceramics) were seriously considered for the baseplate and other major structural components. Cost and convenience ruled this out.

Measure-and-compensate methods are used to correct the interferometer readings for the effects of temperature gradients.

When we combine the effects of all of the trade-offs and compensations we come to the conclusion that the later accuracy,  $\delta x$ , depends on the total temperature excursion  $\Delta t$  during the total writing time,  $t_w$ , according to

$$\delta x \approx \alpha \Delta T t_w \quad . \quad (16)$$

Here the proportionality constant  $\alpha$  is about  $0.1 \mu\text{m}/^\circ\text{C}$ . Time enters in as a further drift problem. Thus there can be a drift in the reference to which the room temperature is compared. We believe that this is not significant during any one working day.

In a future and more-expensive system we could obtain significant improvements by:

- o A temperature controller with greater stability and
- o Use of low expansion ceramics wherever possible. This could lead to roughly a factor of two improvement.

#### 4.3 Stage Motion

As the stage micrometers are driven, the stage itself undergoes periodic up and down motion from the gear drive. This motion is certified by the manufacturer to be  $\pm 1 \mu\text{m}$ . The primary effect is not on focus (our depth of focus is around  $25 \mu\text{m}$ ) but on the demagnification ratio

$$m = S_o/S_I \quad , \quad (17)$$

where  $S_o$  = object distance and  $S_I$  = image distance for the demagnifying microscope. The relative error in  $m$  is

$$\frac{\delta m}{m} = \frac{\delta S_o}{S_o} + \frac{\delta S_I}{S_I} , \quad (18)$$

where  $\delta S_o$  and  $\delta S_I$  are the errors in  $S_o$  and  $S_I$ . Stage motion of  $\delta S_I = 1 \mu\text{m} = 10^{-4}$  cm leads to a relative magnification error

$$\delta m/m = \delta S_I/S_I \approx 5 \times 10^{-3} . \quad (19)$$

This gives  $\delta m/m = 5 \times 10^{-3}$  for  $S_I = 1.9 \times 10^{-2}$  cm. Note that changing  $m$  leads to a change in the fringe position because we are writing a field of nominal size  $200 \mu\text{m}$ . Thus  $\delta m/m = 5 \times 10^{-3}$  leads to a maximum error of  $1 \mu\text{m}$  in fringe resolution.

When we attempt to drive the stage to a new position, we arrive at a location  $x_s, y_s$  which differs from the target position  $x_t, y_t$  by unpredictable errors  $\delta x$  and  $\delta y$ . That is

$$x_s = x_t + \delta x \quad (20)$$

and

$$y_s = y_t + \delta y . \quad (21)$$

These errors are the settling errors certified to be roughly  $10 \mu\text{m}$ . Our approach to dealing with these errors is to

- o Measure  $x_s, x_t$ ,
- o Calculate  $\delta x, \delta y$ , and
- o Write the CRT image

laterally displaced from the center by  $\delta x/m$ ,  $\delta y/m$ . The demagnified image is then automatically centered on  $x_t, y_t$ .

#### 4.4 Photographic Plate Choice

The photographic plate must be extremely flat to achieve good resolution because of the previously-noted demagnification effect. Kodak offers the flattest available photographic plates (Microflat®). These have a flatness of  $\delta S \approx 4 \mu\text{m}$  over the full usable aperture of 7 cm and thus limit writing accuracy on fringe width due to the plate (as explained in Section 3.3) to 4  $\mu\text{m}$ .

In photographic emulsions big grains are used to gain high speed. Because we want high resolution ( $\sim 5 \mu\text{m}$ ) we must expect low speed. Lower speed means longer exposures. Longer exposures means less resolution. Clearly there is a narrow "window" in the set of all emulsions which satisfies a mutually-consistent, useful tradeoff between speed and resolution. Of the few potentially-interesting emulsions, only one was available on Microflat plate. We conclude that this was the only commercially-available photographic plate suitable for use with this hologram writer.

#### 4.5 CRT Choice

The CRT choice is dominated by considerations of speed and distortion. To avoid writing the hologram a point at a time we chose to write it a square cell at a time. The speed improvement factor in so doing is the number of points in the cell. The ultimate speed, of course, would come from writing the whole hologram at once. For the number of points and for the positional accuracy we require, this ultimate CRT does not exist. The question then is how large a cell (in terms of number of resolvable elements) can we write to the required accuracy. Our original goal was to write fringes to  $\lambda/100$

accuracy. With a fringe period of  $10 \mu\text{m}$  this requires  $0.1 \mu\text{m}$  on the hologram. On the CRT it requires  $p/50$  accuracy across the cell, where  $p$  is the width of a single point. That is, we need to confine the cell to that region of the CRT giving less than 2% distortion. For a band CRT the cell may be very small. For the best CRT, it may be very large. For the good and affordable CRT we chose the Infodex PD1200M34 with a 12 cm diameter RCA C82200 ESI tube. The usable area was 5 cm x 5 cm for our purposes.

The image must be "on" long enough to expose the emulsion. We hope it is bright enough so that retrace is not required to achieve the desired exposure level. The phosphor decay time would be less than the time needed to step the stage and let it settle to within  $0.1 \mu\text{m}$ . For our system that time is 0.17 seconds. The decay time for the RCA tube phosphor is 0.001 seconds.

The chief obstacle to better CRT performance (bigger cells) is cost. The next best CRT was roughly \$5,000 more than the one we bought. In a program in which cost was a prime consideration, this was not a serious option.

#### 4.6 Mirror Design

The right angle mirror attached to the stage to allow stage x-y position monitoring must be locally-flat to allow the interferometer to function. In addition it must be accurately  $90^\circ$  in order to not couple x and y measurements. Suppose it is accurately  $90^\circ$ , we can align the mirror at  $x = x_0$  and adjust the mirror alignment so that the x indication is constant to better than  $0.1 \mu\text{m}$  regardless of y. The test is to move to a much different value of x and scan y there. It should again lead to "constant" x. If the angle is not  $90^\circ$  but  $90^\circ + \delta\theta$ , then the maximum "coupling error" is

$$ce = \ell \delta\theta$$

(22)

where  $\ell$  is the maximum scan distance (around 8 cm in this system). Thus we would like to have  $ce < 0.1 \mu\text{m}$  or

$$\delta\theta < 10^{-5} \text{ cm}/8 \text{ cm} = 1.25 \times 10^{-6} \quad . \quad (23)$$

Microradian accuracy over 8 cm is extremely hard to achieve (or even verify). Testing in the visible across the whole face gives a diffraction limit of

$$\Delta\theta \sim \lambda/\ell = 0.5 \times 10^{-4}/8 \sim 5\delta\theta \quad . \quad (24)$$

It follows that we can not expect to avoid correcting  $x$  according to  $y$ , i.e. calibrating the mirror and storing a simple correction factor for use by the computer.

#### 4.7 Vibration

In a system designed to approach  $0.1 \mu\text{m}$  positional accuracy, normal vibrations would be catastrophic. We have taken four precautions to minimize vibration. First, we have used an air-suspended table to isolate the system from normal slow vibrations (people walking, machinery operating, earth settling, etc.). Second, we have used a granite table to damp fast vibrations. Third, we have used only heavy, solid components. Fourth, we write holograms only after disturbances from stage motion and disturbances from human operators have had time to dampen out.

#### 4.8 Air Currents

The temperature controlled room continually circulates air. This should maintain the desired temporal and spatial uniformity, but it can also cause

sufficient turbulence to cause misdirection of the writing beam. We have built turbulence-spoiling shields to remove this problem.

#### 4.9 Interferometer

The interferometer was one of the easiest choices. What we sought was

- o 0.1  $\mu\text{m}$  resolution or better
- o reading speed sufficient to verify damping of stage motion in a small time.

The standard of the industry is the Hewlett-Packard interferometer we chose. It is more than adequate on both counts.

#### 4.10 Radio-Frequency Interference

We anticipated that radio frequency interference (RFI) would present a problem for our delicate display circuitry and tried to shield the environmentally-controlled room against it. It turned out that RFI also affected the controlling PDP 11/23 computer. After much effort, this and a line surge problem caused by the room controls was brought under satisfactory control.

#### 4.11 Information Flow

We needed to accomplish two primary tasks by computer:

- o Calculation of the hologram (a nontrivial task in that the writing beam must be fed information to 0.1  $\mu\text{m}$  accuracy over an 8 cm diameter hologram for a total of about  $5 \times 10^8$  bits), and
- o Control the writing (move the stage, sense stage position, write the cell, decide next cell position, obtain cell data, etc.).

In principle, one computer could do both tasks. In practice, this proved far too expensive.

To operate the holowriter at its design speed while making fringe calculations on-the-fly, Aerodyne's PRIME computer would have to be devoted full time to the task (all other users banned for the entire writing time). The financial burden to the program of this operation would have been immense. We chose, instead, to split the tasks between two computers by providing a dedicated PDP 11/23 to control the holowriter. The primary cost (in time, inventiveness, and dollars) this approach caused was that an interface between the computers had to be designed and built and a 100 foot special cable had to be designed and installed to connect the computers. A simplified task division is shown in Figure 4.1.

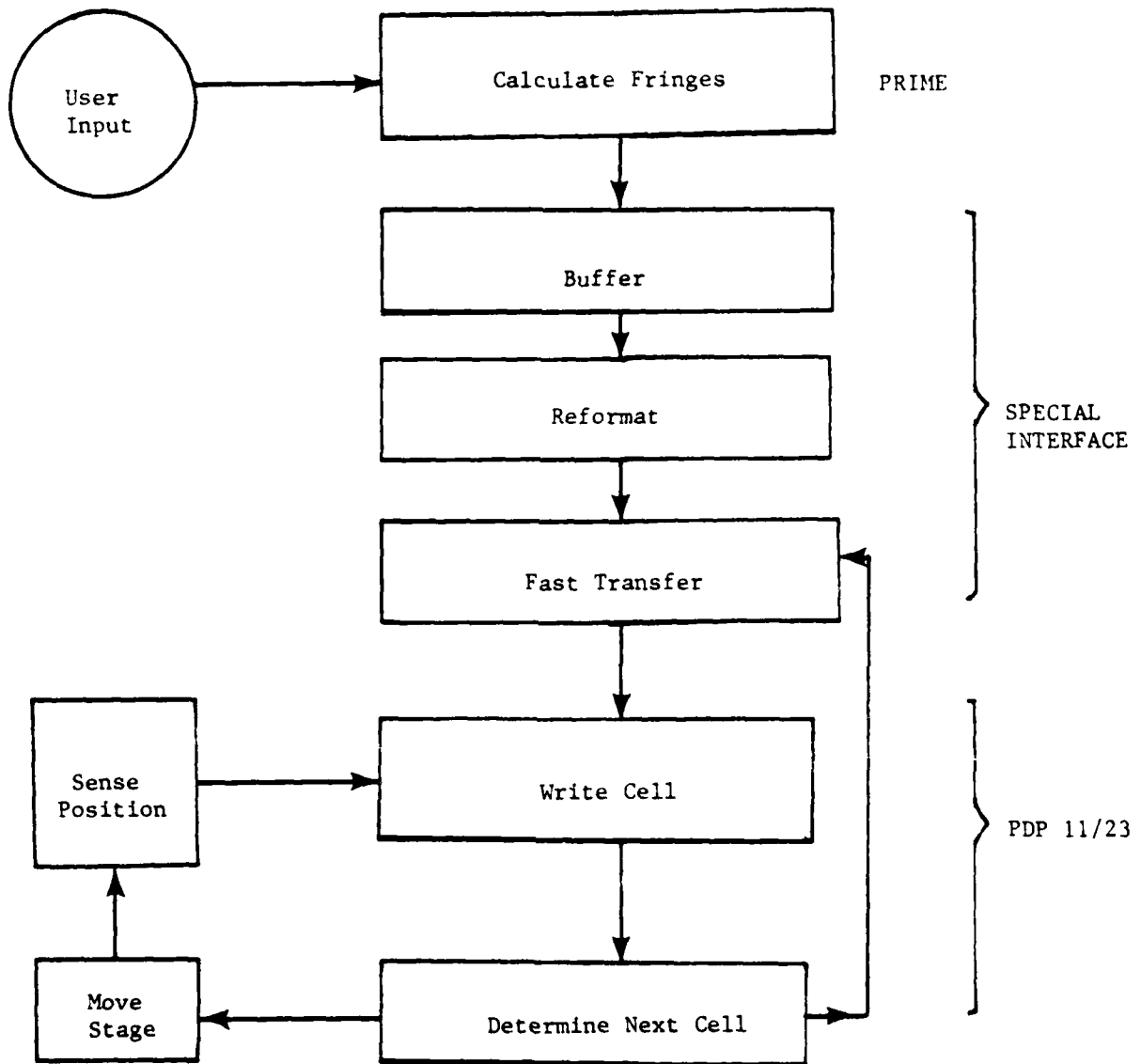


Figure 4.1. Simplified Information and Control Flow Diagram.

## 5. SYSTEM DESCRIPTION

### 5.1 Introduction

Having described the system philosophy, the system components, and the system design parameters, we turn now to the description of the system as a whole. In a sense, the system was designed once the components were selected. Unfortunately most of the hard work went into assembly and integration.

### 5.2 System Appearance

Figure 5.1 shows the CRT, mount optics, stepping motors, and interferometer on the granite, air-suspended table in the environmentally-controlled room. The room environment is set, controlled, and recorded with the equipment shown in Figure 5.2. Two entries to the room are locked during hologram writing (Figure 5.3). This room had to have all light leaks plugged and all control lights covered because the plate is panchromatic and is exposed for a multihour period. All manual manipulations after the plate is removed from the box are done in darkness using an infrared viewer. Outside the second door of the primary double-chambered entry way (Figure 5.4) is the PDP 11/23 and associated I/O equipment. The operator controls all operations from here. Down the hall is the PRIME computer (Figure 5.5) used for the fringe calculations and the interface based on the PRIME/RAMTEC interface (Figure 5.6) which was already designed for rapid data transfer from the PRIME.

### 5.3 Alignment, Magnification, and Focus

Plates are inserted in the dark (as noted above) and kinematically located within the plate holder. The location of the first fringe is selected

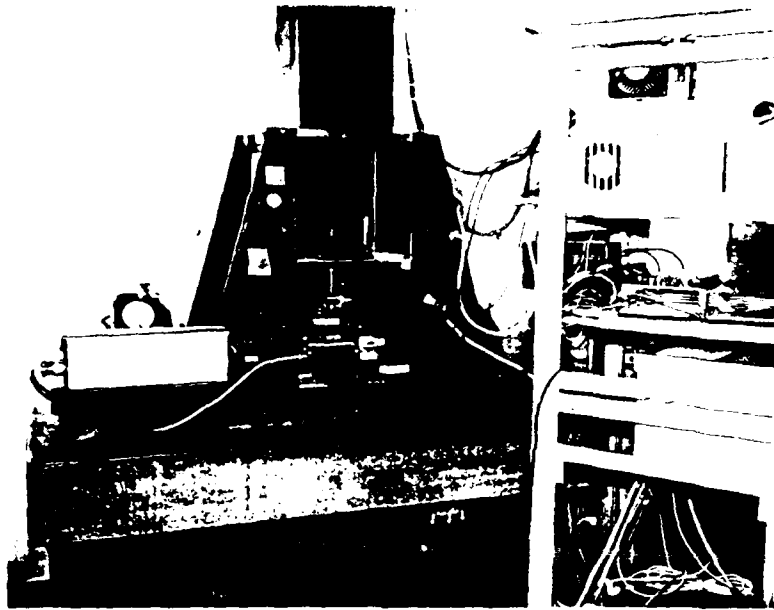


Figure 9.1. The ORI, Microscope, and Detector system are shown here on the Air-Suspended Particle Index. The rack on the right is in the instrumentation portion of the central electronics.



Figure 5.2. Environmental Control Stations.

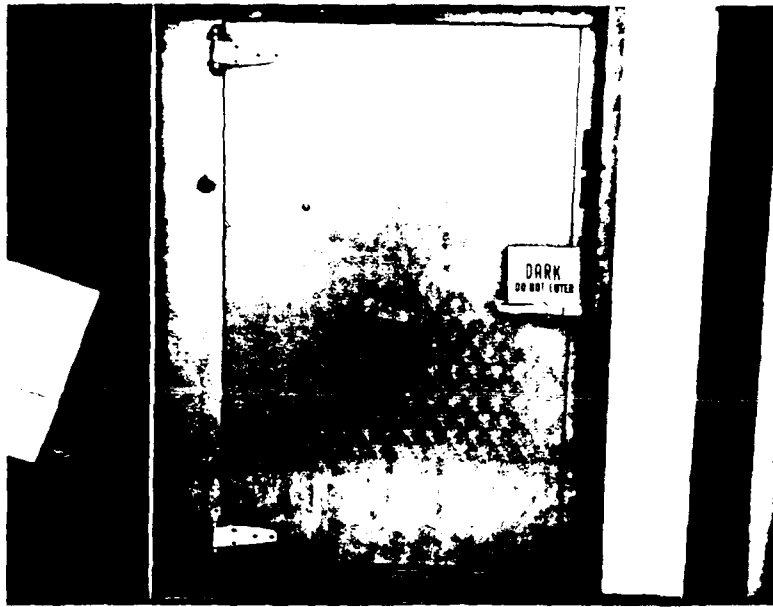


Figure 5.3. One of the Insulated Metal Doors to the Temperature Controlled Room.

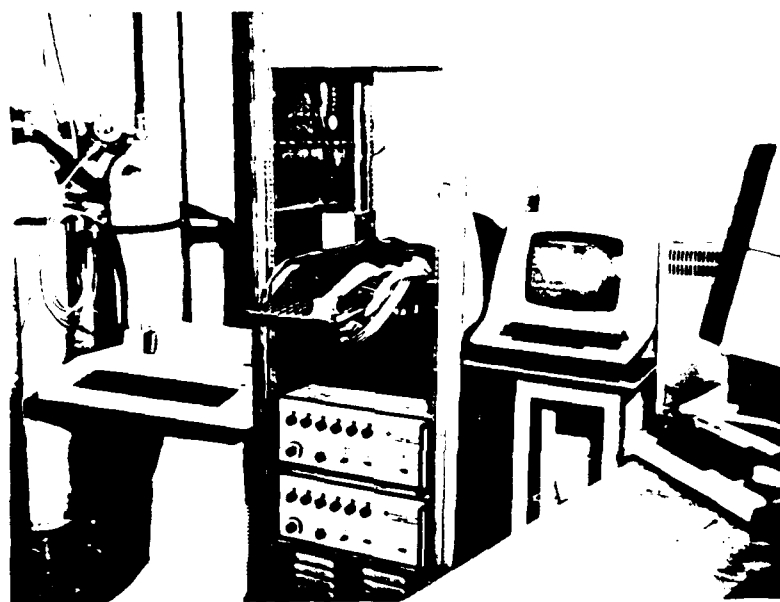


Figure 5.4. Adjacent-To-The-Room Electronics.



Figure 5.5. Aerodynes Prime 400 Computer System.



Figure 5.6. The Ramtek Display (a) is interfaced to the Prime Through Special Boards Designed and Built at ARI. A single panel of additional electronics (b), converts that interface to the required high data rate Prime PDP 11/23 interface.

by the starting point on the micrometers on the stage motion transducers. The magnification can be "trimmed" electronically. By exposing square cells which ought to abutt perfectly while changing the magnification electronically between cell exposures, we can achieve agreement between the cell size on the plate and the interferometrically-controlled stage motion. Thus the scale of the cell can be accurate to interferometric accuracy. Focus can be obtained through direct observation of backscatter through the pellicle beam splitter. It has proved satisfactory in practice to:

- o Align the plate holder apparatus once optically so that no focus change occurs over the whole plate,
- o Measure the air gauge gap indicator reading, and
- o Use the air gauge to reset the focus for new plates (the microscope must be elevated and reset in the dark to insert a new plate).

#### 5.4 Final System Specifications

Table 5-1 shows final system performance levels.

Table 5-1 - Final System Performance Levels

Parameter	Value
Hologram Size	7 cm x 7 cm
Fringe Size (Minimum)	5 $\mu\text{m}$
Absolute Location Accuracy	0.15 $\mu\text{m}$
Writing Time (Full Format)	12.5 hours

#### 5.5 Time Budget For One Cell

Table 5-2 shows the time required for the various operations.

Table 5-2 - Time of the Writing of a Single Cell

Operation	Time (milliseconds)
Step	170
Expose (2 traces)	100
TOTAL	270

#### 5.6 Sample Rulings

Figure 5.7 shows a 7 cm x 7 cm Ronchi ruling with 10  $\mu\text{m}$  lines. Figure 5.8 shows a magnified area covering several cells. This illustrates the accuracy and quality now achievable.



Figure 5.7. A 7 cm x 7 cm Ronchi Ruling Written with the Holowriter.

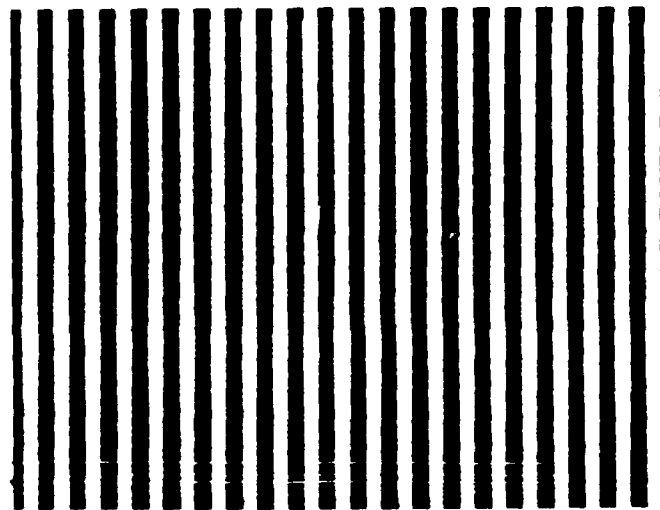


Figure 5.8. A Magnified Image of a Portion of the Figure 5.7 Hologram Showing 10  $\mu\text{m}$  Lines.

APPENDIX A  
DETAILED PROCEDURE FOR CALCULATING THE GMF

We describe here the detailed procedure which would allow any interested reader to generate his own GMF's.

We chose to work with a 128 x 128 grid, but this choice was arbitrary. We could go larger or smaller. Binary numbers are necessary for doing fast Fourier transforms (FFT's).

The GMF algorithm\* works with sampled values of the FFT at all points in the filter plane. Our program allows us to work with either the actual sampled points or with a mean and Gaussian variance calculated from them. We chose the latter approach. Thus, for each of 128 x 128 points, we calculate and store the mean and variance of FFT's at that point the associated various inputs scenes (in this case, rotated and magnified aircraft).

The FFT's will have both real and imaginary parts. We treat them as independent 128 x 128 matrices. The real matrix generates the real part of the GMF and the imaginary matrix generates the imaginary part.

We do not need to calculate the 2 x 128 x 128 GMF values simultaneously. We can break them up arbitrarily and get the same result because we are assuming (precisely for this immense calculational advantage) that values at each of these points are independent of the values at any other. We chose to run the 256 rows (of 128 points each) sequentially and store the resulting values of the "weights" s coefficients in the GMF.

Actually, what we calculate in this way is not the GMF but its complex conjugate. Thus, to obtain the correlation pattern for any input scene, we:

---

\*The Actual algorithm is Program 360A-CM-03X from the IBM SYSTEM/360 Scientific Subroutine Package (1970), p. 52.

- (1) Perform an FFT (128 x 128) on that scene,
- (2) Multiply the FFT by the GMF, and
- (3) Inverse FFT the product.

Thus, the GMF is used exactly as the matched filter is.

If we write

$$\text{GMF} = \text{FFT}^* [p(x,y)] \quad ,$$

then

$$p(x,y) = \text{FFT}^{-1} [\text{GMF}^*] \quad .$$

Here,  $p(x,y)$  is the pattern to which the GMF is matched. As shown in Figure 2-11,  $|p(x,y)|$  looks somewhat like an edge-enhanced, blurred image of an airplane.

## APPENDIX B

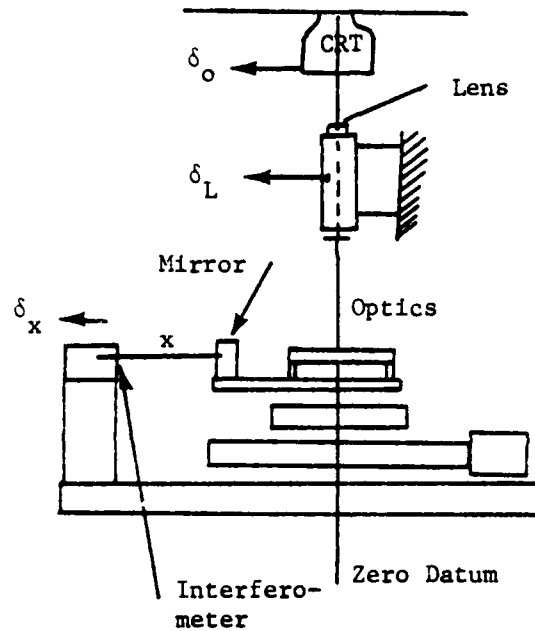
### Thermal Expansion Compensation

The attached analysis is a summary of the final design for the subject equipment.

The materials and geometry were chosen for thermal expansion symmetry at the center of the carriage stroke. Plus and minus errors will occur at the extremes of carriage stroke. Also, the compensation was based on uniform bulk temperature changes of the structure.

For the foregoing reasons, two of the the Hewlett-Packard  $\pm 0.05^{\circ}\text{F}$  sensors (#10563AOPT-001) were located to monitor the temperature of the base and the aluminum spacer.

Geometry



Motion of elements is referenced from zero datum at optical center line.

- $\delta_o$  = object displacement (CRT)
- $\delta_L$  = lens displacement
- $\delta_x$  = interferometer displacement

The displacement error ( $\delta_i$ ) of the image is:

$$\delta_i = \frac{\delta_o}{m} = \frac{\delta_o}{250}$$

For the CRT

$$\delta_i = \delta_L \left(1 + \frac{1}{m}\right)$$

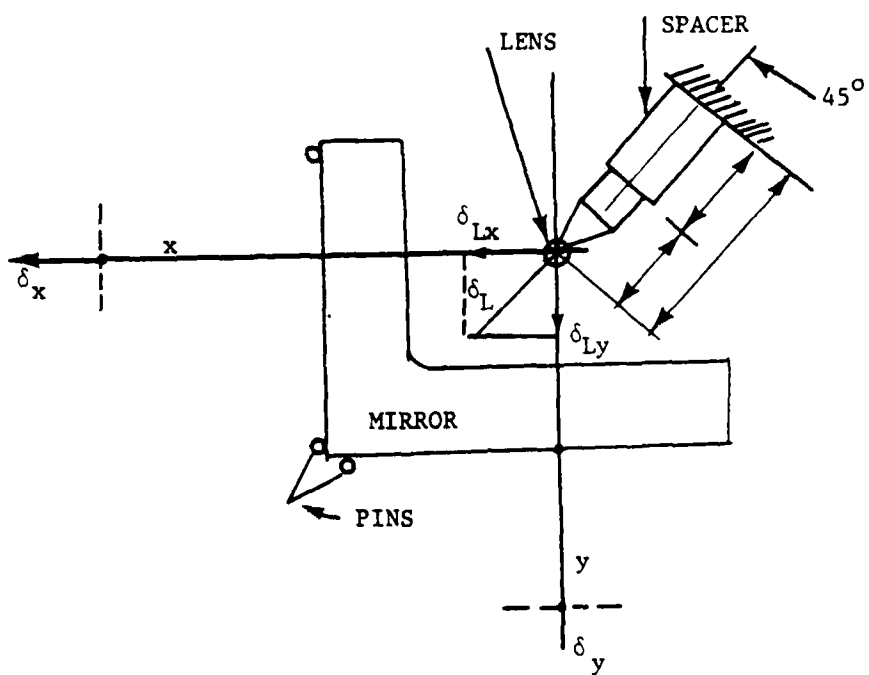
$\delta_i = 1.007 \delta_L$  For the lens

$$\delta_i = \delta_x$$

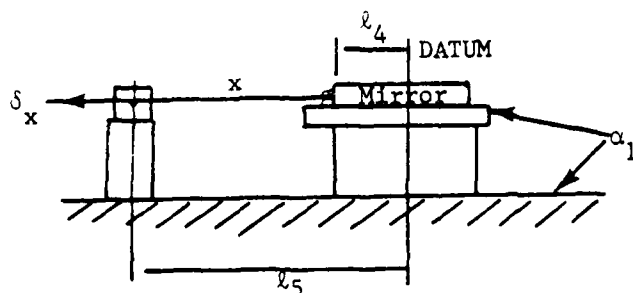
For the interferometer

Thus, thermal motion of the interferometer and lens is critical. The CRT is no problem.

Material Compensation In x-y Plane



Interferometer ( $\delta_x - \delta_y$ )



$\alpha_1 = 5.5 \times 10^{-6}/^{\circ}\text{F}$  for 410  
stain. steel.

$y = x = 6.44''$  at center position.

With mirror spring loaded to locating pins, the change in interferometer reading is  $\delta_x = \Delta t \alpha_1 (l_5 - l_7)$  or

$$\delta_x = x \Delta t \alpha_1 \qquad \delta_x = \delta_y = 6.44 \times 5.5 \times 10^{-6} = 35.4 \text{ microinches}/^{\circ}\text{F}$$

This has the effect of moving the stage  $\delta_x = \delta_y$  relative to the spatial datum.

Lens Motion ( $\delta_L$ )

For uniform, bulk t of the structure, we can select the lens spacer to compensate for  $\delta_x - \delta_y$ . From diagram:

$$\delta_{Lx} = \delta_{Ly} = \delta_L \sin 45^\circ \text{ and we want}$$

$$\delta_x = \delta_{Lx} \text{ for compensation so}$$

$$\delta_L = \frac{\delta_x}{.707} = \frac{35.4}{.707} = 50 \text{ microinches}/^\circ\text{F required, and}$$

$$\delta_L = \Delta t (\ell_2 \alpha_2 + \ell_3 \alpha_3 - \ell_1 \alpha_1) \quad \begin{aligned} \alpha_1 &= 5.5 \times 10^{-6}/^\circ\text{F} \\ \alpha_2 &= 10.6 \times 10^{-6} \text{ for lens} \\ \alpha_3 &= 13.10^{-6}/^\circ\text{F for alum} \end{aligned}$$

$$\delta_L = \Delta t [2.75 \times 10.6 + 13 \ell_3 - \alpha_1 (\ell_3 + 2.75)] \quad \ell_2 = 2.75 \text{ fixed}$$

$$\delta_L = \Delta t [29.2 + 13\ell_3 - 5.5\ell_3 - 15] \quad \ell_1 = \ell_2 + \ell_3 = \ell_3 + 2.75$$

$$\delta_L = \Delta t [14 + 7.5\ell_3] \text{ and we want } \delta_L = 50 \text{ microinches}/^\circ\text{F, so}$$

$$\ell_3 = \frac{50 - 14}{7.5} = 4.8'' \text{ and } \ell_1 = 7.55 \text{ inches}$$

APPENDIX C

Photographic Plate

The high speed holographic plates from Kodak (Type 131-02) on Microflat plates were the only satisfactory plates. Relevant catalog data is attached.

A hologram is formed by recording the interference pattern of coherent light waves, as either amplitude or phase variations in a recording medium. Typically, one of the waves is either a plane wave or a divergent spherical wave and it is known as the reference beam. The other wave usually reflected from an object under study, is referred to as the signal beam. When the processed hologram is reilluminated by its original reference beam, its original signal beam will be reconstructed in both amplitude and phase because of a hologram's unique reversal property. Conversely, when reilluminated by the more complicated signal beam, the hologram will reconstruct a somewhat modified but similar reference beam. This is used in complex spatial filtering. Ideally, holographic materials should have the following proper-

ties: resolution greater than the spatial frequency of the hologram's interference pattern; very low grain noise; dimensional stability; realtime development without processing; erasability for reuse; no thickness limitations; and high sensitivity at popular wavelengths. A number of materials combine some of these properties, but none has them all.

When selecting the material most suitable to your needs, the two most important considerations are resolution and sensitivity. However, in particular applications the supporting substrate, emulsion thickness, granularity, maximum contrast density, and cost may all be important. The charts on the opposing page will help you select the proper material for your application. Film prices are on page 94.

**SUBSTRATES:** The primary substrates used to support holographic emulsions are glass plates, acetate sheeting, and polyester sheeting. Glass plates, being the most rigid and stable, can be held in a variety of holders and be precisely repositioned after development. Holographic films in roll or sheet format are less expensive, but difficult to hold stationary for long exposures. Polyester bases (such as the Kodak ESTAR) are strong and dimensionally stable but, unfortunately, they exhibit birefringence which may pose problems in some applications such as coherent optical data processing. For these applications, acetate base films are recommended. If an emulsion is not available on glass substrates, we advise that you use a vacuum film holder, or simply sandwich the film between two glass plates.

**EXPOSURE:** A primary parameter used to compare holographic film is the exposure energy (ergs/cm<sup>2</sup>) required to produce a hologram with a neutral density (D) of 1.0. Generally, in amplitude holograms, maximum diffraction efficiency occurs between D = 0.6 and 0.8. However, in processes where phase holograms are generated by bleaching the image, a slightly higher exposure level is required. Obtaining the best exposure is normally a trial and error series of tests. However, with the use of the NRC Model EM-1 Exposure Mask (pg. 80) six exposures are obtained simultaneously on a single plate and thus saves time and money in selecting the optimum exposure for a particular application.

**RESOLUTION:** A commonly used parameter to compare the resolution of photographic film is termed the "resolving power". This value (in lines/mm) is obtained by photographing Target Objects with Contrasts (TOC) of either 1,000:1 (high) or 1.6:1 (low). The recording of holographic fringes is, however, a different process. It has been found that holograms were obtained even when the fringes generated by the signal and reference beams have spacings two to three times smaller than that of the photographic resolving power for a given film. Nevertheless, for the sake of providing a common reference point, the photographic resolving power has been used here in the chart.

**SHRINKAGE:** Because it causes a grating spacing change, emulsion shrinkage has undesirable effects. For example, shrinkage of transmission hologram emulsions causes small image distortions resulting in spurious fringes in real-time interferometry. Unfortunately, shrinkage cannot be completely eliminated, since voids are always created when unexposed silver-halide grains are removed during fixing. However, some success has been reported filling these voids with chemicals. Of all the emulsions listed in the film selection table, Kodak SO-173 appears to shrink the least.

**GRANULARITY:** Photographic emulsions are fine silver-halide crystals dispersed in a gelatin binder. After processing, the ex-

posed grains become globules or filaments of metallic silver, that introduce a certain amount of undesired scattering. The granularity values in the film selection table are 1,000 times the standard deviation of density about D=1 when scanned by a microdensitometer having a circular aperture of either 48 mm or 6 mm. However, because of the very low granularity of holographic emulsions, reliable measurements are often hindered by instrument noise.

**CONTRAST:** Since most holographic materials have uniformly small grains, photographic contrast is high. When low contrast is desired, you can use either special developers or simply lower the developer concentration, temperature and development time. The contrast values (γ) shown in the film selection table identify the

KODAK PRODUCT	EXPOSURE TO ACHIEVE				
	HeCd 3250	HeCd 4416	Ar 4880	Ar 5145	Nd:YAG 5320
High Resolution Plate, Type 1A Film SO-343 (E7B); 649GH (E4AH)	(400)	1000	1500	1000	800
High Resolution Plate, Type 2A Spectroscopic Type 649-F Plate/Film	(1000)	3000	2500	2000	2000
Holographic Plate, Type 120-02/Film SO-173		500	—	—	—
Mincard II Film, SO-424/SO 141	20	80	50	50	100
[REDACTED]	20	80	50	50	100
High Speed Holographic Film, SO-253		20/35	40/65	25/35	20/30
High Speed Holographic [REDACTED] 131-02 [REDACTED]			40/65	25/35	20/30
Direct Positive Laser Recording Film, SO-285		35	45	55	75
Recordak Direct Duplicating Print Film, 5468, 8468	5	100	100	50	40
High Definition Aerial Film, 3414	0.4	0.6	3	2	2
Technical Pan Film SO-115		0.4	0.8	0.8	0.7
Linagraph Sheilburst Film 2474/2476	0.15	0.09	0.3	0.3	0.2
2479 RAR Film	0.1	0.05	0.2	0.3	0.2
2475 Recording Film	0.07	0.03	0.06	0.07	0.06
2485 High Speed Recording	0.03	0.007	0.04	0.05	0.04
AGFA-GEVAERT					
[REDACTED]	—	[REDACTED]	30	20	20
8375 Plates	—	150	1500	250	250
10E75 Plate/Film	—	60	300	120	60

slope of the straight line portion of the characteristic (D vs. log E) curve (H-D curve) and assumes development times in normally recommended developers at 20°C with frequent agitation.

**EMULSION THICKNESS:** For most applications, emulsion thickness is not a factor. However, a thicker emulsion is required either when multiplexing or when making reflection holograms. Emulsion thickness is greater in glass plates than in film and may result in slightly different holographic performance.

**STANDARD BASE:** The codes used in this column of the film selection table are as follows:

- "BKD"-----Backed with an anti-halation coating
- "UNB"-----Does not have anti-halation coating (unbacked)
- "E"-----ESTAR polyester substrate
- "A"-----Acetate substrate
- "B"-----Dyed gelatin peiloid backing applied to substrate

- "CB"-----Clear gelatin peiloid backing applied to substrate
- "C"-----No backing applied to substrate
- "AH"-----Support has 0.1 neutral density in the substrate

The numbers indicate the glass substrate thickness (ex. 0.040UNB 040 is thick plate, unbacked) or the thickness of the film substrate (ex. E4B ESTAR base is 4 mil thick dyed gelatin peiloid backing).

**PROCESSING:** Almost all photographic materials listed here can be processed with readily available Kodak D-19 and Rapid Fixer. Since residual silver-halide grains cause noise, it is important to thoroughly fix the plates and films. To quickly dry after washing, immerse in 50%-70% alcohol for one minute and blow dry with a clean air jet. The Kodak Type 120 and 131 exhibit a residual dye stain following normal processing. This stain can be removed by bathing the holograms for 1 to 3 minutes in a 75% methanol solution following normal washing.

APPLICATIONS / LASER	ARGON	He-Ne; KRYPTON	RUBY
TRANSMISSION HOLOGRAPHIC DISPLAY	10E56 649F* SO424 125	SO173 120 SO253 131	10E75 8E75
REFLECTION HOLOGRAPHIC DISPLAY	649F* 10E56	120 10E75 649F*	8E75
HOLOGRAPHIC INTERFEROMETRY	SO424 125 10E56	SO253 131 10E75	10E75
REAL-TIME HOLOGRAPHIC INTERFEROMETRY	NRC Photopolymer H2	NRC Photopolymer H1	NRC Photopolymer H1
HOLOGRAPHIC OPTICAL ELEMENT	649F* HRP	120	8E75
LASER DATA RECORDING	HRP** SO424 125	SO173 120	8E75
COMPLEX SPATIAL FILTERING	HRP**	SO173 120	8E75
SPATIAL FILTERING	Linagraph Shellburst	Linagraph Shellburst	Linagraph Shellburst
SPECKLE PHOTOGRAPHY	SO424 125 10E56	SO253 131 10E75	Not Applicable
LASER ILLUMINATED PHOTOGRAPHY	Linagraph Shellburst	Linagraph Shellburst	Linagraph Shellburst

\* 649F Plates Converted to Dichromated Gelatin. Call NRC for procedure.  
649F\* is the only material with a flat spectral response for full color reflection holograms.

D = 10/ergs.cm <sup>2</sup>			RESOLVING POWER @ TOC /1000 l/1.6 μ	GRANULARITY @ D = 10 48 μm 6 μm	CONTRAST	EMULSION THICKNESS	AHU	STANDARD BASE	DEVELOPMENT		
HeNe 6328	Kr 647	RUBY 6943									
-	-	-	2000+	<5 <10	8	6 Plates 7 Film	No No	0060 BKD E75 64-AH	6-8 HRP/D-19 6-8 D-19		
-	-	-	2000+	<5 <10	5	6	No	060 UNB	6-8 HRP/D-19		
900	900	5000+	2000+	<5 <10	5/4	176	No	0040 UNB E4AH	6-8 D-19		
400	400	400	2000+	<5 <10	5/4	6	No	0040 UNB E4B	6-8 D-19		
-	-	-	1250	630	<5	13	4	<3	No	A5CB/E4C	6-8 D-19
-	-	-	530	<5	13	4	7	No	0040 UNB	6-8 D-19	
5/8	3.5/6	1000+	1250	800	<5	14	7	No	E4B	6-8 D-19	
5/8	3.5/6	1000+	800	<5	14	7	9	No	0040 UNB	6-8 D-19	
30	50	-	1250	530	<5	14	2	<4	Yes	A5C	5 D-19
-	-	-	1000	400	<5	17	19	3	No	A5C, A7C	5 D-19
2	2	5	630	250	9	33	0.08-2.4	<4	No	E2.5B	D-19, D-76
0.4	0.3	-	320	125	8	-	1-3	7.5	No	E4AH	6-8 HC-110(D) 4 D-19
0.15	0.15	2.5	125/160	50/63	24/22	-	0.5-2	-	No/Yes	E4B/E4AH	D-19 D-76
0.08	0.08	0.5	100	40	24	-	0.5-1.8	-	Yes	E4AH	D-19, D-76
0.05	0.05	0.05	63	22	32	-	0.4-2	-	No	E4AH	D-19 DK-50
0.03	0.03	0.04	50	20	47	-	0.9-1.8	-	No	E4AH	857 D-19
-	-	-	1500+	-	-	-	7	7.5	No	0050/A5	5 D-19
75	75	50	200+	-	-	-	3	7	No	0050	5 D-19
20	20	20	1500+	-	-	-	4	7.5	No	0050/A5	5 D-19



For holographic nondestructive testing and similar real-time applications, the NRC H-Series Photopolymer provides rapid-access recording with high resolution. The two important advantages over conventional recording media are: (1) the exposed hologram can be viewed instantaneously without processing, and (2) the cost per shot can be low for volume users. Exposures can be made with argon, helium-neon, or ruby laser light, depending on the spectral sensitization chosen.

Photopolymer recording materials consist of a solution of acrylate monomers, a catalyst, and a dye sensitizer. Sensitized dye molecules, when excited by laser light, react with the catalyst to produce free radicals that initiate polymerization of the acrylate monomers. Therefore, the liquid photosensitive material becomes a plastic solid after exposure. Image information is stored via modulation of the thickness and index of refraction of the polymer and thus is classified as a phase rather than an amplitude recording material. In comparison to Kodak 649F plates, the photopolymer is about two orders of magnitude less sensitive but has up to 10 times higher diffraction efficiency. This allows a corresponding increase in the relative power in the reference beam to reduce the exposure time accordingly.

**PREPARATION:** The photopolymer is shipped in two containers. Prior to mixing, the individual solutions are quite insensitive to

light and have long shelf life. After mixing, the light-sensitive liquid is spread between two glass plates to form an approximately 10  $\mu$ m thick layer. The material is held in place by surface tension when placed vertically in a plate holder.

**SPECTRAL RESPONSE & SENSITIVITY:** The photopolymer is available in two spectral sensitizations:

PHOTOPOLYMER H-1 He-Ne and Ruby laser wavelengths

PHOTOPOLYMER H-2 Argon laser at 488 nm line

The energy required for exposure is 4 to 5 mJ/cm<sup>2</sup>. One-fourth of that energy can be provided by pre-exposing or biasing with an incoherent light source. After exposure, the hologram can be temporarily fixed by incoherent light or permanently fixed by heating to 150°C for 10 seconds.

**RESOLUTION AND IMAGE QUALITY:** Nonlinearity of the image approaches that of an ideal phase hologram. With a resolution of between 2,000 to 3,000 lines/mm, image contrast of 40 to 1 can be obtained. In addition, approximately 20% of the peak diffraction efficiency is accessible within 0.1 sec. Initially, the hologram may appear milky, but after a short period of time will become clear.

**PRICE:** Available in two sizes: 25 ml-----\$60.00  
100 ml-----\$150.00

NRC is a dealer in both Kodak and Agfa-Gevaert products for holography and laser photography and is stocking certain materials for your convenience. All materials are stored under the proper conditions prior to shipping. Suggested list prices are as of August, 1977 and subject to revision without notice.

Shipment from stock, quickly to anywhere in the continental U.S.A.

## GLASS PLATE

### Kodak

649F	2 x 2 in. x 0.040 in., 36 per box \$52.20
649F	2 x 2 in. x 0.040 in., Backed, 36 per box \$57.60
649F	2 x 2 in. x 0.060 in., Precision 36 per box \$88.20
649F	2 x 2 in. x 0.060 in., Precision Backed, 36 per box \$91.80
649F	4 x 5 in. x 0.040 in., 36 per box \$73.80
649F	4 x 5 in. x 0.040 in., Backed, 36 per box \$81.00
649F	8 x 10 in. x 0.040 in., 12 per box \$64.20
120-02	2 x 2 in. x 0.040 in., 36 per box \$52.20
120-02	2 x 2 in. x 0.060 in., Precision, 36 per box \$188.20
120-02	4 x 5 in. x 0.040 in., 36 per box \$73.80
120-01	4 x 5 in. x 0.040 in., Backed, 36 per box \$81.00
120-02	4 x 5 in. x 0.250 in., Microflat, 6 per box \$59.70
120-02	5 x 7 in. x 0.250 in., Microflat, 6 per box \$60.00
120-02	8 x 10 in. x 0.040 in., 12 per box \$64.20
131-02	2 x 2 in. x 0.040 in., 36 per box \$52.20
131-02	4 x 5 in. x 0.040 in., 36 per box \$73.80
131-01	4 x 5 in. x 0.040 in., Backed, 36 per box \$81.00
131-02	8 x 10 in. x 0.040 in., 12 per box \$64.20
125-02	2 x 2 in. x 0.040 in., 36 per box \$52.20
125-02	4 x 5 in. x 0.040 in., 36 per box \$73.80
125-01	4 x 5 in. x 0.040 in., Backed, 36 per box \$81.00
125-02	8 x 10 in. x 0.040 in., 12 per box \$64.20
125-01	8 x 10 in. x 0.040 in., Backed, 12 per box \$70.80
HRP-2	4 x 5 in. x 0.250 in., Microflat, 6 per box \$25.00
HRP-2	5 x 7 in. x 0.250 in., Microflat, 6 per box \$30.65

### Agfa-Gevaert

8E75NAH	4 x 5 in., 12 per box \$14.75
8E75AH	4 x 5 in., Backed, 12 per box \$16.20
8E75NAH	8 x 10 in., 6 per box \$19.10
8E75AH	8 x 10 in., Backed, 6 per box \$21.00
10E56NAH	4 x 5 in., 12 per box \$14.75
10E56AH	4 x 5 in., Backed, 12 per box \$16.20
10E56AH	8 x 10 in., Backed, 6 per box \$21.00
10E75NAH	4 x 5 in., 12 per box \$14.75
10E75AH	4 x 5 in., Backed, 12 per box \$16.20
10E75NAH	8 x 10 in., 6 per box \$19.10
10E75AH	8 x 10 in., Backed, 6 per box \$21.00

## SHEET AND ROLL FILM

### Kodak

649F	35 mm x 100 ft, A5B Acetate Base, SP414, Unperf \$70.80
SO-115	4 x 5 in., 50 per box \$12.30
SO-173	4 x 5 in., 25 per box \$25.20
SO-173	35 mm x 150 ft, SP417, Perf \$52.45
SO-173	9.5 in. x 200 ft, SP983, Unperf \$466.30
SO-173	12 in. x 150 ft, SP983, Unperf \$442.80
SO-253	4 x 5 in., 25 per box \$25.20
SO-253	35 mm x 150 ft, SP417, Perf \$52.42
SO-253	70 mm x 150 ft, SP474, Unperf \$103.40
SO-424	4 x 5 in., Minicard II, 50 per box \$12.00
SO-424	35 mm x 100 ft, Minicard II, SP417, Perf \$14.00
2474	4 x 5 in., Linagraph Shellburst, 25 per box \$5.95
2476	35 mm x 150 ft, Linagraph Shellburst, Backed, SGE417, Perf \$20.05

### Agfa Gevaert

10E75NAH	70 mm x 100 ft, Unperf \$44.95
10E56AH	70 mm x 100 ft, Unperf, \$44.95

APPENDIX D

Hologram Display Generator

Attached is the manual on the hologram display generator created specially for this program.

## 1.0 INTRODUCTION

The Hologram Display Generator is part of a larger system designed to produce large format, high resolution holograms on glass photographic plates by a step and repeat method. The purpose of the HDG is to generate single frame images on a CRT which are imaged on the photographic plate. Data describing the image are transferred in compressed form from a LSI 11 computer.

This manual includes a description of the requirements imposed on the HDG by system constraints, a functional description of the HDG hardware, and an explanation of the microcode used to satisfy these requirements.

A single hologram consists of about 300 by 300 frames. Each frame has a resolution of 2000 pixels by 800 scan lines resulting in a total information content of  $1.4E11$  pixels. This fact dictates 3 important characteristics of the HDG: high speed, efficient data encoding, and reliability.

## 2.0 REQUIREMENTS

The function of the Hologram Display Generator (HDG) is to accept compressed data describing a given type of hologram from the system LSI 11 computer and to generate the requisite signals to display the information in expanded form on an Infodex high resolution display system.

The image to be generated on the display comprises a series of bars of varying width and constant brightness which are parallel to one axis of the display. The image is formed in a raster and the bars are defined in terms of their widths in one direction (X) and in number of raster lines in the orthogonal direction. The image is formed in a 50 mm by 50 mm square approximately in the center of the 5 inch diameter CRT. For purposes of this system, the format represents 2000 pixels in the X direction and 800 scan lines in Y. The image can be moved +/- 10 percent in any direction, so the useful (or used) portion of the screen is 60 mm by 60 mm corresponding to 2400 pixels by 960 scan lines.

The signals required to drive the display are X and Y deflection voltages and a binary unblanking signal. The information transferred from the LSI 11 computer includes digital words describing the position of the origin of the image (XOFFSET, YOFFSET), the size of the image on the CRT (XMAG, YMAG), the number of scan lines in each group of bars (LRPT), a control/status word (CSR), and a block of data of up to 1024 words describing bar widths.

The time required for a single scan line is 52 microseconds which includes 30 microseconds of active scan time, 6 microseconds for the sweep to stabilize, and 16 microseconds for retrace. The time to generate a single cell (one complete raster), if all 800 lines are used, is 41.6 milliseconds.

The X and Y deflection amplifiers in the display are identical and have input impedances of about 1000 ohms and deflection factors of about .5 inches per volt at the input. The unblanking amplifier has an input impedance of 50 ohms and a required voltage swing of 0 to -3.5 volts where 0 volts corresponds to a blanked condition. The display has a front panel brightness control, so brightness need not (indeed, cannot) be controlled by the HDG.

The display is located in a controlled environment chamber. Because of the speed and precision of the signals between them, the HDG is located adjacent to the display. The computer is located outside the controlled chamber about 20 cable feet away.

### 3.0 DETAILED DESCRIPTION

The major elements of the HDG are shown in the block diagram in Figure 1. Interface elements between the HDG and the Infodex display and the LSI 11 computer are evident in the block diagram. The memory is used to store the block of data describing bar widths. These descriptors are converted to an unblanking signal by the counter and delay circuits and the number of scan lines in a bar is counted in the line repeat counter. The various HDG circuits are controlled by a microcontroller in accordance with a ROM stored program.

#### 3.1 LSI 11 Interface

The interface between the HDG and the LSI 11 computer includes a Programmed I/O port for transferring the single word information and a DMA port for transferring the block of words describing bar widths.

The PIO interface is split between a quad width wire wrap board located in the computer and the main HDG circuit board. The two are connected by two 20 foot ribbon cables. The base address and the interrupt vector address are selectable with switches on the quad board and are currently set at octal 767700 and 0 respectively. (Although interrupts are not used now, they are available for future use.) The defined addresses and their descriptions are as follows:

<u>SIGNAL</u>	<u>ADDRESS</u>	<u>DESCRIPTION</u>
CSR	Base	Control/status word. Bit 0:RLRST - A zero in this bit stops HDG controller and sets program to address 0. A one enables HDG operation. Read/write.  Bit 1:Page - Selects program from either page 0 or page 1 of ROM. Read/write.  Bit 2:Not used.  Bit 3:STEXP/ - Starts exposure sequence when raised to a one. Should be held at zero until all descriptors have been passed from LSI 11, then raised for at least 1 instruction cycle. Must be returned to zero before next DMA transfer is complete. Read/write.  Bit 4:Not used.  Bit 5:ENAST - Enable interrupt A. Read/write.

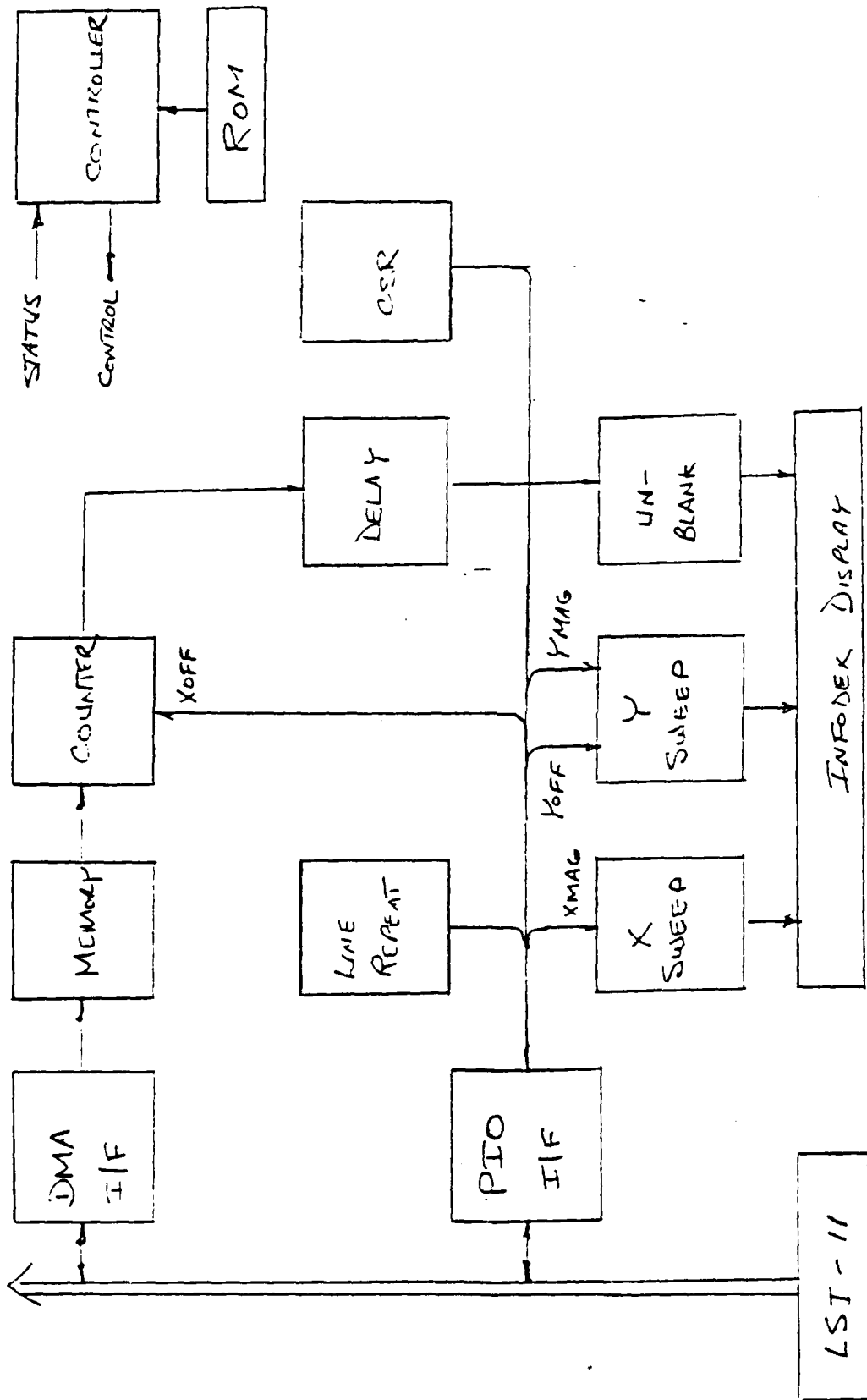


Figure 1 - IIG Block Diagram

Bit 6:ENBST - Enable interrupt B.  
Read/write.

Bit 7:RQSTA - Interrupt request A.  
Not currently used. Read only.

Bit 8:ECC - End of cell bit indicates  
when one for more than 10 microsec-  
onds that a complete cell has been  
written. May be one for less than 10  
microseconds at end of individual  
scan lines. Read only.

Bits 9 through 14:Not used.

Bit 15:RQSTB - Interrupt request B.  
Not currently used. Read only.

XOFF	Base+2	X offset in pixels in bits 0-11 in two's complement format. Write only
YOFF	Base+4	Y offset in scan lines in bits 0-9 in positive true format. Write only
YMAG	Base+10	Y magnification factor in bits 0-7. Value of 128 (decimal) represents nominal magnification factor. Values of 255 and 0 repre- sent approximate changes of +/- 10 percent. Write only
LRPT	Base+12	Number of scan lines per bar group.LRPT equals two's com- plement of (scan lines + 1). Bits 0-9 only. Write only.
XMAG	Base+14	X magnification factor in bits 0-7. Write only.

The DMA interface consists of a DEC DRV11B interface board in the computer and complementary circuitry on the HDG board. As with the PIO interface, the two are connected by two 20 foot ribbon cables.

The DMA base address can be set with switches on the DRV11B board and is currently set at octal 772410. The registers in the DRV11B of interest here are the word count register (WCR) at the base address, the bus address register (BAR) at the base address plus 2, and the

control/status register (CSR) at the base address plus 4. Details of DRV11B operation can be found in the appropriate DEC documentation; knowledge of this information is assumed in the following discussion.

The LSI 11 computer signals the HDG when it ready to make a DMA transfer by dropping the READY line. The HDG, when it reaches the appropriate point in its cycle, examines the READY line and, as soon as it is found low, starts the DMA transfer. The transfer proceeds in the single cycle mode as fast as the computer will permit. There is no further intervention by either the computer or the HDG until the WCR overflows, thus raising the READY line and terminating the operation. With the current version of the HDG program, the READY line is monitored by the HDG and other tasks are suspended until it rises. A transfer of 1024 words ( the size of the HDG memory) takes about 3.5 milliseconds

The data are transferred to the HDG in a word format and input directly to the HDG memory. The HDG interface generates memory address increment and memory write signals automatically.

Although only one way data transfer is required (computer to HDG), there is provision for transferring information from the HDG memory back to the computer for diagnostic purposes. This is done by raising the FNCT 1 bit (bit 1) in the DRV11B CSR.

Circuitry is included for testing single word parity during a computer to HDG transfer. The parity bit is bit 13 of each word and may be either even or odd depending on the condition of jumpers on the HDG circuit board. The jumpers are currently set for even parity. The parity test is selected by raising the FNCT 2 bit (bit 2) in the DRV11B CSR. Upon detection of a parity error, the HDG will raise the ATTN signal (bit 13) which will in turn set the ERROR bit (bit 15), terminate the transfer, and generate an interrupt if the interrupt enable bit (bit 6) is set.

The remaining function and status lines available on the DRV11B are not used.

### 3.2 Memory

The memory is arranged in a 1024 x 16 bit configuration and includes a memory address counter and an address return register. The address counter can be reset, preloaded from the return register, or incremented by a HDG controller instruction. The counter is incremented automatically during a DMA operation after each word transfer. The return register can be loaded with the contents of the address counter with a controller instruction. Write signals to the memory are generated by the interface circuitry during a DMA operation.

Bar widths are stored sequentially starting at location 0. Bits 0-11 of each word represent bar width in a two's complement format. Bit 15 is a 1 if the corresponding bar is to be unblanked. The cumulative value of bar widths in any group must total at least 2400 pixels less

the value of the X offset. The cumulative value of all the bar widths except the last in a group must be less than 2000 pixels. Meeting these criteria ensures that the last descriptor in a group will be active at the end of each scan line. Failure to meet these criteria will result in misregistration between bar groups.

The last word in a block of cell descriptors, following the last bar width in the last bar group, signifies the end of cell with a 1 in bit 14.

The remaining bits (12,13) are not used.

### 3.3 X Deflection

The X deflection signal is generated by an integrating sawtooth generator synchronized with a counter. The counter circuit has 2 counter chains which are driven by a stable 10 MHz clock and count up to 0 from preset values. Additional circuitry generates 2 signals, called SW and XVAL, which are used to synchronize the other parts of the HDG. The SW signal controls solid state switches in the feedback path of an integrating amplifier. When SW is 1, the switches are open and the integrator generates a ramp waveform. When the switches are closed, the waveform retraces rapidly. SW is high for 36 microseconds and low for 16 microseconds. These values can be changed in 100 nanosecond increments by changing jumpers on the HDG circuit board.

The XVAL signal rises 6 microseconds after the SW signal and falls simultaneously. XVAL defines the useful sweep time. The 6 microsecond hiatus between SW and XVAL provides time for the sweep waveform to become stable and linear.

Because deflection repeatability is important, the X sweep runs continuously and covers the full 2400 pixel format. Offset of the origin in the X direction is achieved by appropriate blanking at the beginning and end of each line rather than by moving the entire pattern.

The reference signal used to drive the integrator is provided by a precision reference voltage conditioned by the XMAG word via an 8 bit D/A converter. The result is a reference signal which can be varied by the XMAG word by +/- 10 percent in steps of 1 part in 256.

Trim controls have been provided to vary the nominal scale factor, the gain of the XMAG word, the nominal X center value, and the value of the reference voltage.

### 3.4 Y Deflection

The Y deflection circuitry includes a 10 bit line counter, a 10 bit D/A converter, magnification control circuitry, and an output amplifier.

The counter can be reset, incremented, or loaded with the Y offset

word from the LSI 11 under microprogram control. With a range of 10 bits, up to  $1024$  raster lines can be addressed. The pattern is offset to accommodate positioning tolerances by preloading the counter with the Y offset word (YOFF). Subsequent lines are addressed by incrementing the counter one line at a time.

The D/A converter is a 12 bit unit with the 2 least significant bits tied to zeroes. As with the X sweep, the reference drive is derived from a precision voltage source conditioned by the YMAG word. Full scale variation of the YMAG word will cause a  $\pm 10$  percent change in the reference signal in steps of 1 part in 256.

The output amplifier is the same as in the X axis. It is capable of driving a 50 ohm load at  $\pm 5$  volts and has a bandwidth in excess of 50 MHz.

Trim controls have been provided to vary the nominal pattern size, position offset, magnification factor, and reference voltage.

### 3.5 Unblanking

The CRT image is generated by converting the bar width descriptors to time delays in synchronism with the X sweep and using the resulting signal to turn the CRT beam on and off.

The bar width conversion circuitry includes 2 counter chains for the coarse timing and a variable delay circuit for the fine timing. The bar width descriptors, which are stored sequentially in the memory, are 12 bit numbers in two's complement notation specifying the number of pixels in each bar. The 2 least significant bits control a delay circuit which, at the appropriate time, generates a delay of 0, 12.5, 25, or 37.5 nanoseconds corresponding to 0 through 3 pixels. The remaining 10 bits are used to preset the counters.

The counters are used alternately; while one is counting, the other is being loaded with the next bar descriptor. The active counter is selected by an EVEN/ODD flip flop that is toggled at the end of each count sequence, thereby transferring control to the opposite counter. Both counters are enabled or disabled simultaneously by the CNTEN flip flop which is set or cleared by the controller. The counters are clocked by a 20 MHz clock and advance from their preset values till they overflow and a carry signal is generated. The carry signal resets the counter, triggers the delay circuit, toggles the EVEN/ODD flop, and sets a status flip flop monitored by the controller. The opposite counter is enabled immediately and proceeds to count on the next rising edge of the 20 MHz clock.

The 2 least significant bits have, prior to the advent of the carry signal, been buffered in latches and decoded to select 1 of 4 possible delay paths. The carry signal is propagated through the selected path and, at the other end, clocks, into a flip flop, bit 15 of the bar descriptor, corresponding to the value of the next bar, i.e. 1 or 0 indicating blanked or unblanked.

The unblanking signal at the output of the flop is buffered and

converted to a voltage swing of 0 to -3.5 volts with an impedance of 50 ohms to drive the Z input of the Infodex display.

When the controller detects a carry signal indicating counter overflow, it executes the steps necessary to prepare the disabled counter for the next sequence. This includes incrementing the memory and loading the counter and delay buffer. These activities require about 400 nanoseconds (4 instruction cycles) so bar widths smaller than 32 pixels (12.5 ns per pixel) cannot be accommodated.

When one counter overflows, the other starts counting on the next 20 MHz clock cycle irrespective of the value of the delay. To prevent truncation error, which will accumulate if not corrected, a modified bar width is generated by subtracting the time delay associated with the previous bar from the current bar width. It is this modified width, rather than the value directly from memory, which is directed to the counter and delay circuits.

### 3.6 Line counter

In a given hologram, all bars are a predetermined size in the Y dimension. This size is specified by the Line Repeat word (LRPT) transmitted from the LSI 11 via the PIO interface and maintained in a 10 bit counter. The line repeat counter can be reset, incremented, or loaded with the LRPT word by the controller. The carry bit of the counter can be monitored by the controller to indicate overflow. Because the counter cannot be decremented, LRPT must be in a two's complement format.

### 3.7 Controller

The HDG controller operates on a 32 bit microword in accordance with a PROM stored program at a cycle rate of 10 MHz. It can issue control signals, monitor the status of input signals, and branch in response to programmed conditions.

Two types of branch are permitted: a tabular branch and an unconditional branch. In the unconditional branch mode, when a selected status signal becomes true, the program branches to a previously specified location. In the tabular branch mode, the bit pattern formed by the condition of a group of status signals is OR'd with a base address to yield a branch location.

The microword is divided into 4 groups of 8 bits each. Bits 0 through 7 specify the address of the next instruction or the base address of a tabular branch instruction.

Bits 8 through 15 are mask bits used to select status signals for examination. The lower 5 bits of the group are AND'd with 5 status signals to form a tabular branch word.

<u>BITS</u>	<u>SIGNAL</u>	<u>DESCRIPTION</u>
0	CRY1	Carry from counter 1. Must be cleared by CLRCRY.
1	CRY2	Carry from counter 2. Must be cleared by CLRCRY.
2	CRY3	Carry from counter 3. Must be cleared by CLRCRY.
3	CRY	Carry from any of above. Must be cleared by CLRCRY.
4	READY	Goes high when DMA READY line goes low.

Table 1 - Tabular Branch Codes

The upper 3 bits are decoded to select 1 of 7 status signals (or none of the 7) to be monitored for an unconditional branch. Both types of branching can be used in a single instruction. If the unconditional branch status is false, the tabular branch is executed. If the unconditional branch status becomes true, the unconditional branch is executed.

<u>CODE</u>	<u>SIGNAL</u>	<u>DESCRIPTION</u>
20	RUN	False when DMA is active
40	LNCRY/	True when line repeat counter overflows
60	XVAL	False during X sweep
80	XVAL/	True during X sweep
A0	YCRY/	True when Y sweep counter overflows
C0	STEXP/	True when bit 3 of CSR is true
E0	EOC/	True when End of Cell line (bit 14 of bar width descriptor) is true

Table 2 - Unconditional Branch Codes

Bits 16 through 23 define function codes which are decoded to generate control signals. The upper and lower nibbles are decoded separately into 15 lines each plus NOP's. By specifying functions in both nibbles, 2 control signals can be generated in a single 100 nanosecond instruction cycle.

<u>CODE</u>	<u>MNEMONIC</u>	<u>DESCRIPTION</u>
<u>NIBBLE 1</u>		
0	NOP	No operation
1	MR	Maser reset
2	LDCNTO	Load odd counter
3	LDCNTE	Load even counter
4	LDDLY	Load delay buffer
5	LDLC	Load line repeat counter
6	INCL	Increment line repeat counter
7	RSTL	Reset line repeat counter
8	BMSET	Enable beam on
9	STEVEN	Set EVEN/ODD flag to even
A	DMAST	Start a DMA transfer

NIBBLE 2

0	NOP	No operation
1	MARST	Memory address reset
2	MAENB	Store memory address
3	LDM	Recall memory address
4	INCM	Increment memory address
5	CNTON	Enable counters
6	CNTOFF	Disable counters
7	Not used	
8	LDAD	Load branch address
9	YRST	Reset Y counter
A	YLD	Load Y counter with YOFF
B	YCNT	Increment Y counter
C	LDXOFF	Load XOFF into counters
D	CLRCRY	Clear the carry flags

Table 3 - Function Codes

Bits 24 through 31 specify the location of the branch address in an unconditional branch instruction. The branch address can be issued in any instruction before or including the branch instruction.

The program memory has a capacity of 512 words divided evenly into 2 pages. The page is selected by bit 1 of the HDG CSR word. Controller programs cannot operate over the page boundary.

The controller is enabled by RLRST (bit 0 of the HDG CSR word). When RLRST is 0, the controller is disabled. When RLRST is driven to a 1, the controller starts operating at location 0 of the selected page.

#### 4.0 MICROCODE

Following are flowcharts and coding sheets describing the HDG microcode. Each block on the flowchart corresponds to a single instruction. The numbers to the left of the blocks refer to instruction addresses.

The program has several nested loops which are executed with varying frequency. Instruction 01 is encountered only at initial turn on. Instructions 02 through 0B (between entry points 4 and 1) are executed once per cell. The loop starting at 0C occurs once every  $n$  lines where  $n$  corresponds to the specified number of line repeats. The loop starting at 0E is executed every line. Most of the action takes place between entry points 2 and 3; this loop is traversed once every two bar widths which, at maximum resolution, results in a loop cycle time of about 1 microsecond.

After a master reset and a memory address reset, the controller waits for the DMA READY line to fall indicating that the LSI 11 is ready for a transfer. During the wait, the BMRST command is continually issued. When the READY line falls, the counters are turned off, the memory address is reset again, the transfer is started, and the branch address for the next instruction is loaded. The controller then monitors the RUN line to determine when the transfer is complete. After the transfer, the program loops until the STEXP/ line falls indicating the LSI 11 is ready for the exposure sequence. Instructions 09 and 0A set the EVEN/CDD flag to even and load the X and Y offsets. Instructions 3B through 3C synchronize the program with the X sweep. The following instruction, 0B, is executed immediately after the start of the retrace.

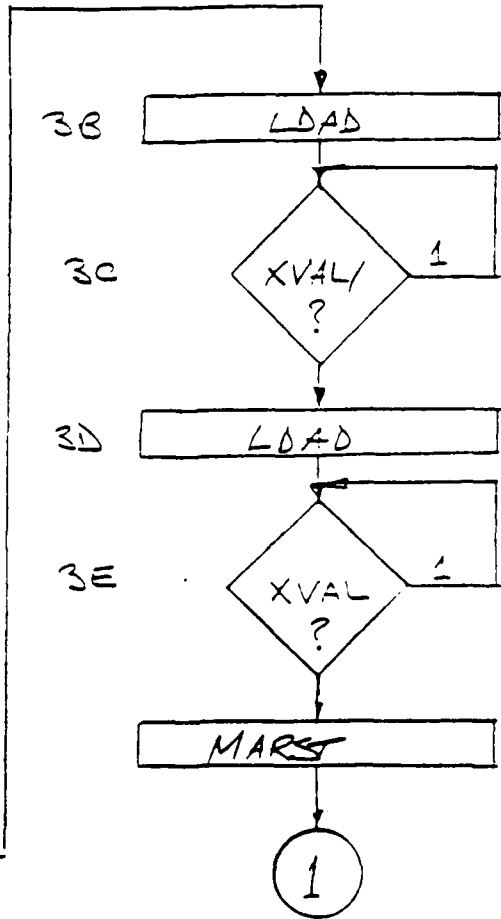
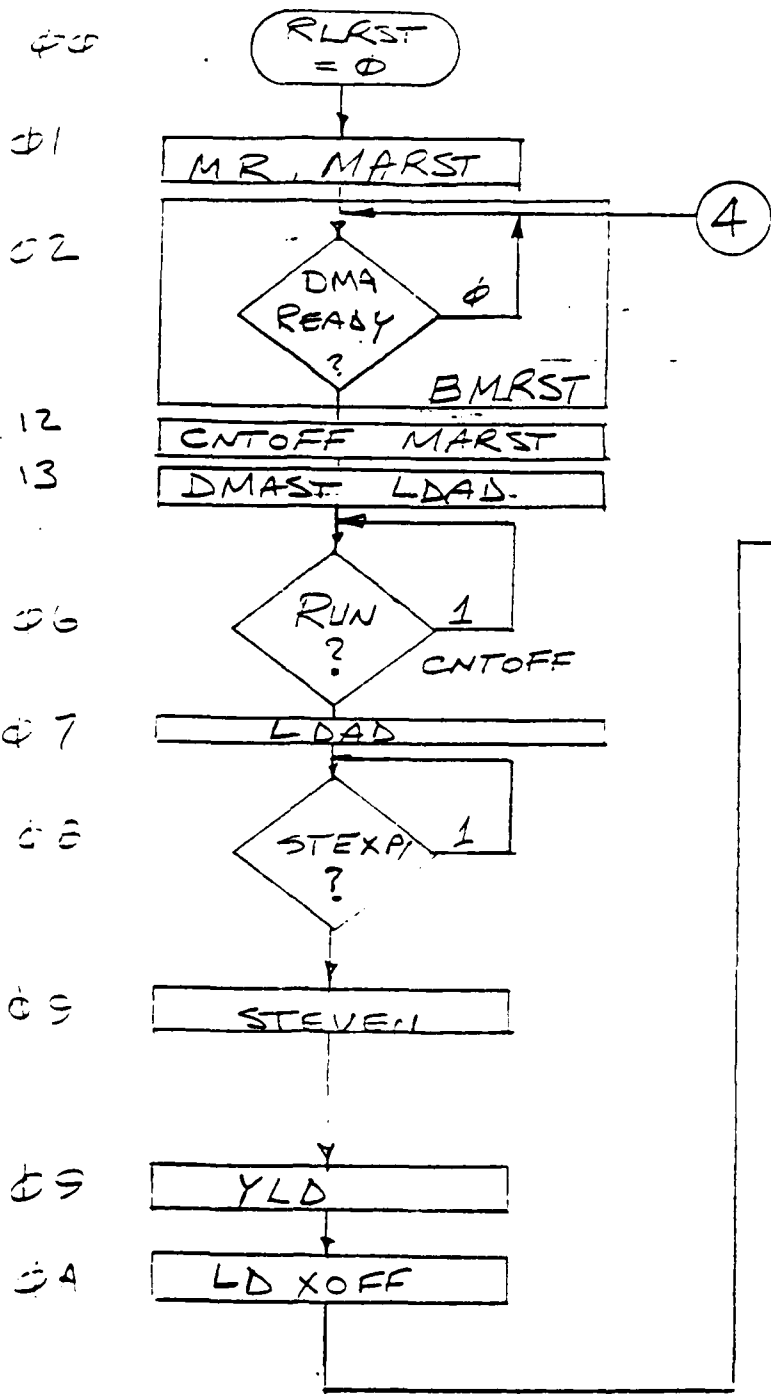
The loop starting at 0C is executed for the specified number of line repeats. At the start of the loop, the memory address is saved so it may be recalled at the start of each line within the group, and the line repeat counter is reloaded with the line repeat count. The loop starting at 0E is executed on each scan line. The timing is such that this instruction occurs during the beginning of the retrace period. So, after loading the X offset, the program loops until the start of the sweep.

The counters are immediately enabled and the unblinking loop, comprising instructions 1A through 22, is entered. This is a continuous loop and is exited only when XVAL falls indicating the end of the forward sweep period and the start of the retrace. This signal is examined in instructions 1C and 20 independently of other loop operations. The remaining instructions set up the counters and delay circuit to measure out the bar widths and shuttle operation between the two counters. At each bar, the program loops until the appropriate counter overflows, then clears the carry flag, loads the delay for the current bar, increments the memory address, and loads the opposite counter. The sequence is repeated as many times as necessary until the scan line is complete.

At the end of each bar, the counters are turned off and the line repeat and Y position counters are incremented. The LNCRY/ line is

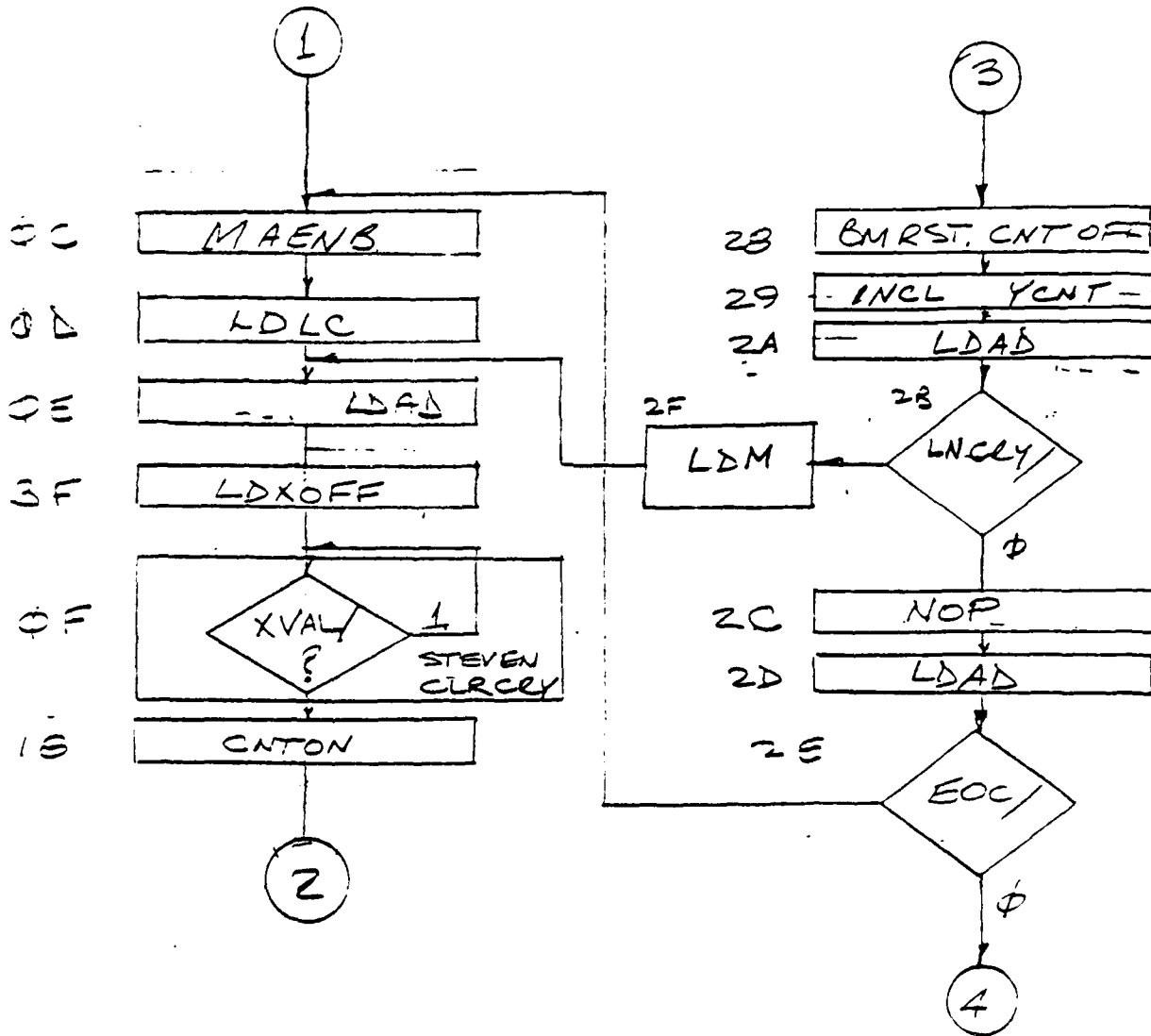
tested to determine if the line repeat counter has overflowed. If not, the previously stored memory address is reloaded into the memory address counter and operation proceeds from instruction OE.

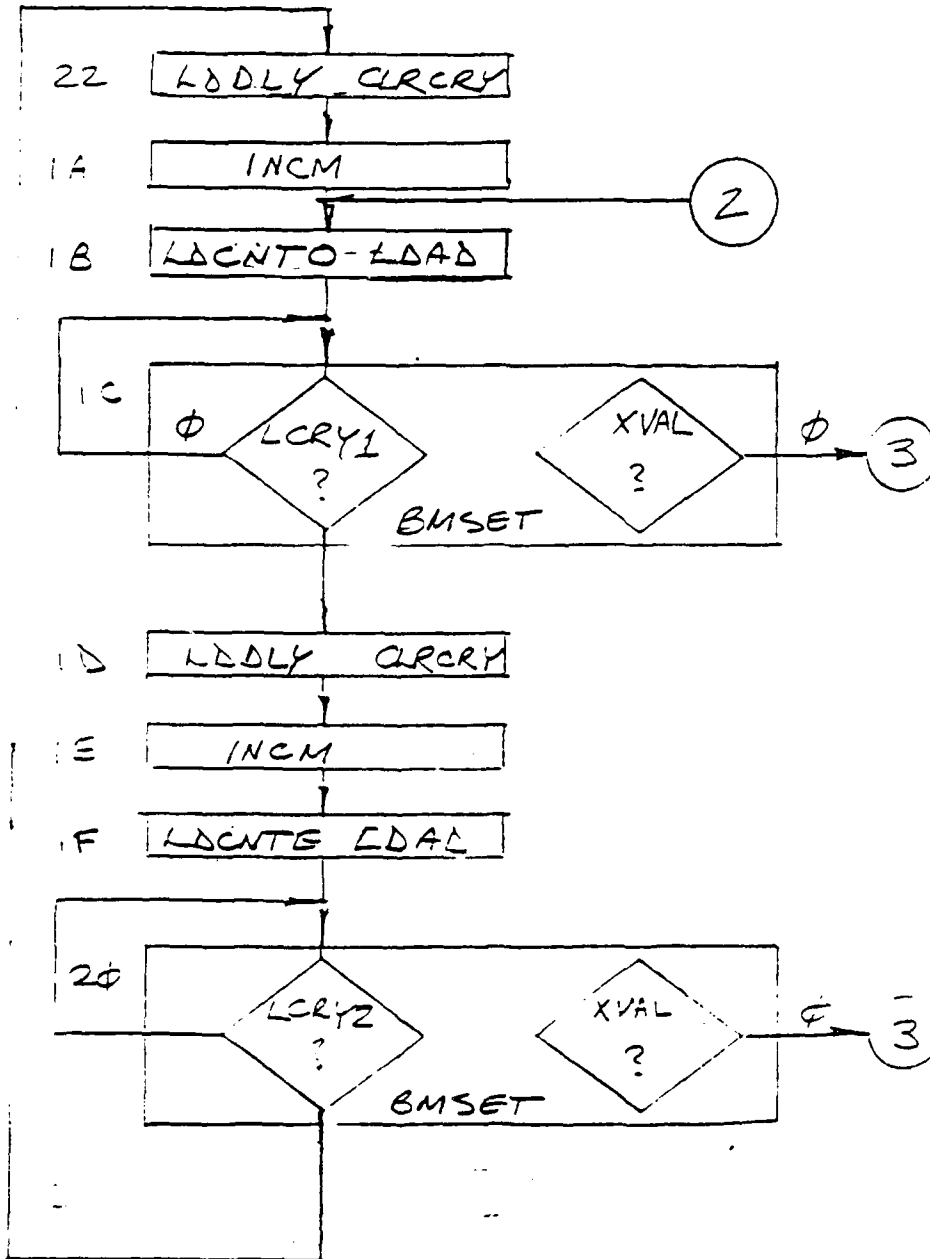
If the line repeat counter has overflowed, bit 14 of the next word in memory is tested to determine if the end of the cell has been reached. If not, the program branches to OC to generate the next group of lines. If it has, control returns to instruction O2 to await the next DMA transfer.



REV 4

FRINGE CODE





ADDRESS	NEXT ADDR	DATA MARK		FUNCTIONS CODE		LIT	FRINGE	1 of 4
		TAB	JUMP	FA	FB			
0	1			P2	FR		FR	
1	2			ΦΦ				
2	3		KEY	ΦΦ				
3				1Φ				
4				-				
5				-				
6	6			2Φ		6Φ	ΦΦ	
7	7			ΦΦ		ΦΦ	ΦΦ	
8	8			ΦΦ		ΦΦ	ΦΦ	
9	9			ΦΦ		ΦΦ	ΦΦ	
A	3B			ΦΦ		ΦΦ	ΦΦ	
B	ΦC			ΦΦ		ΦΦ	ΦΦ	
C	ΦD			ΦΦ		ΦΦ	ΦΦ	
D	ΦE			ΦΦ		ΦΦ	ΦΦ	
E	3F			ΦΦ		ΦΦ	ΦΦ	
F	ΦF			ΦΦ		ΦΦ	ΦΦ	

FRINGE  
 Rev Φ 12/30/81 INITIAL RELEASE

ADDRESS	DATA MEMORY		INSTRUCTION		PC	FRAMES
	PI	TAB JUMP P2	EA	FB		
1	14				17	2 of 4
2	13	φφ			φφ	
3	16	φφ			φφ	
4						
5						
6						
7						
8	1B	φφ			φφ	
9	1A	φφ			φφ	
A	1B	φφ			φφ	
B	1C	φφ			2B	
C	1C	61			φφ	
D	1E	φφ			φφ	
E	1F	φφ			φφ	
F	2D	φφ			2B	

ADDRESS	NEXT ADDR	DATA MARK			FUNCTION CODE			LIT
		TAB	JUMP	P2	FA	FB	FC	
2φ	1P1			P2				
1	2φ			62				11
2	1A			φφ				φφ
3								
4								
5								
6								
7								
8	29			φφ				φφ
9	2A			φφ				φφ
A	2B			φφ				2C
B	2F			4φ				φφ
C	2D			φφ				φφ
D	2E			φφ				φ2
E	φC			Eφ				φφ
F	φE			φφ				φφ

FRINGE = d-1

PAGE ADDRESS	DATA MARK		POSITIONS CODE			LIT
	NEXT ADDR	TAB JUMP	PA	PB	PC	
30	P1		EA	FB	PC	P1
31						
32						
33						
34						
35						
36						
37						
38						
39						
3A						
3B	3C				8φ	3D
3C	3C				4φ	φφ
3D	3E				8φ	φB
3E	3E				3φ	φφ
3F	φF				Cφ	φφ

FRINGE 4 4



*MISSION  
of  
Rome Air Development Center*

*RADC plans and executes research, development, test and selected acquisition programs in support of Command, Control Communications and Intelligence (C<sup>3</sup>I) activities. Technical and engineering support within areas of technical competence is provided to ESD Program Offices (POs) and other ESD elements. The principal technical mission areas are communications, electromagnetic guidance and control, surveillance of ground and aerospace objects, intelligence data collection and handling, information system technology, ionospheric propagation, solid state sciences, microwave physics and electronic reliability, maintainability and compatibility.*

Printed by  
United States Air Force  
Hanscom AFB, Mass. 01731

**DAT  
ILM**